Received: 23 February 2023 | Revised: 29 August 2023 | Accepted: 30 August 2023

DOI: 10.1111/jnc.15962

Journal of Neurochemistry JNC The Official Journal of the International Society for Neurochemistry WILEY

ORIGINAL ARTICLE

Loss of the parkinsonism-associated protein FBXO7 in glutamatergic forebrain neurons in mice leads to abnormal motor behavior and synaptic defects

Jingbo Wang[1] | Sabitha Joseph[1] | Siv Vingill[2] | Ekrem Dere[3,4] | Lars Tatenhorst[5] | Anja Ronnenberg[4] | Paul Lingor[6] | Christian Preisinger[7] | Hannelore Ehrenreich[4] | Jörg B. Schulz[1,8,9] | Judith Stegmüller[1,9]

[1]Department of Neurology, RWTH University Hospital, Aachen, Germany

[2]Max Planck Institute for Multidisciplinary Sciences, Göttingen, Germany

[3]Sorbonne Université. Institut de Biologie Paris-Seine, (IBPS), Département UMR 8256, UFR des Sciences de la Vie, Campus Pierre et Marie Curie, Paris Cedex, France

[4]Clinical Neuroscience, Hermann Rein Strasse 3, Max Planck Institute for Multidisciplinary Sciences, Göttingen, Germany

[5]Department of Neurology, University Medical Center, Göttingen, Germany

[6]Department of Neurology, School of Medicine, Klinikum rechts der Isar der Technischen Universität München, Munich, Germany

[7]Proteomics Facility, IZKF, RWTH Aachen University, Aachen, Germany

[8]Jülich Aachen Research Alliance (JARA)-BRAIN Institute of Molecular Neuroscience and Neuroimaging, Research Center Jülich and RWTH Aachen University, Aachen, Germany

[9]Research Training Group 2416 MultiSenses-MultiScales, RWTH Aachen University, Aachen, Germany

Correspondence
Judith Stegmüller, Department of Neurology, RWTH University Hospital, Pauwelsstrasse 30, 52074 Aachen, Germany.
Email: jstegmueller@outlook.com

Funding information
Deutsche Forschungsgemeinschaft, Grant/Award Number: 368482240/GRK2416, STE1117/10-1 and STE1117/14-1

Abstract

Mutations in *PARK15*, which encodes for the F-box protein FBXO7 have been associated with Parkinsonian Pyramidal syndrome, a rare and complex movement disorder with Parkinsonian symptoms, pyramidal tract signs and juvenile onset. Our previous study showed that systemic loss of *Fbxo7* in mice causes motor defects and premature death. We have also demonstrated that FBXO7 has a crucial role in neurons as the specific deletion in tyrosine hydroxylase-positive or glutamatergic forebrain neurons leads to late-onset or early-onset motor dysfunction, respectively. In this study, we examined NEX-*Cre*;*Fbxo7fl/fl* mice, in which *Fbxo7* was specifically deleted in glutamatergic projection neurons. The effects of FBXO7 deficiency on striatal integrity were investigated with HPLC and histological analyses. NEX-*Cre*;*Fbxo7fl/fl*

Abbreviations: 6-OHDA, 6-hydroxydopamine; C1q, complement 1q; cKO, conditional knockout; Cre, cre recombinase; DAT, dopamine transporter; DOPAC, dopamine, 3,4-dihydroxyphenylacetic acid; DRD1, D1 dopamine receptor; DRD2, D2 dopamine receptor; EDTA, ethylenediaminetetraacetic acid; FBXO7, F-box only protein 7; GABA, gamma aminobutyric acid; GFAP, glial fibrillary acidic protein; HPLC, high pressure liquid chromatography; HVA, homovanillic acid; Iba1, ionized calcium-binding adapter molecule 1; LABORAS, laboratory animal behavior observation, registration and analysis system; MSN, medium spiny neurons; NeuN, neuronal nuclear protein; NEX, neuronal helix-loop-helix protein 1; PBS, phosphate buffered saline; PD, parkinson disease; PET, positron emission tomography; PPS, parkinsonian pyramidal syndrome; SDS-PAGE, Sodium dodecyl-sulfate polyacrylamide gel electrophoresis; SNARE, soluble N-ethylmaleimide-sensitive-factor attachment *protein* receptor); SPECT, *Single photon emission computed tomography*; TH, tyrosine hydroxylase; VGAT, vesicular GABA transporter; VGluT1, vesicular glutamate transporter 1; YKT6, synaptobrevin homolog YKT6.

Jingbo Wang, Sabitha Joseph and Siv Vingill contributed equally to this work.

mice revealed an increase in striatal dopamine concentrations, changes in the glutamatergic, GABAergic and dopaminergic pathways, astrogliosis and microgliosis and little or no neuronal loss in the striatum. To determine the effects on the integrity of the synapse, we purified synaptic membranes, subjected them to quantitative mass spectrometry analysis and found alterations in the complement system, endocytosis and exocytosis pathways. These neuropathological changes coincide with alterations in spontaneous home cage behavior. Taken together, our findings suggest that FBXO7 is crucial for corticostriatal projections and the synaptic integrity of the striatum, and consequently for proper motor control.

KEYWORDS
FBXO7, PARK15, parkinsonism, synapse, synaptopathy

1 | INTRODUCTION

Parkinson disease (PD) and parkinsonism-related disorders have been associated with genetic mutations in *PARK* loci. Among those, mutations in *PARK15* which encodes for FBXO7, have been associated with a recessive and complicated subtype of parkinsonism termed Parkinsonian Pyramidal syndrome (PPS) or PARK15 syndrome (Correa-Vela et al., 2020; Di Fonzo et al., 2009; Jin et al., 2020; Lohmann et al., 2015; Lorenzo-Betancor et al., 2020; Shojaee et al., 2008; Wang et al., 2021; Wei et al., 2018; Yalcin-Cakmakli et al., 2014; Yoo et al., 2020; Zhao et al., 2020). Affected individuals with *PARK15* mutations develop the disease as early as in their teens and present with a wide spectrum of signs and symptoms. The clinical manifestations, described in aforementioned case reports, are characterized by classical PD motor deficits, dysfunctions of the pyramidal tract such as Babinski sign, spasticity and hyperactive deep tendon reflexes. Further symptoms comprise dysarthria, dysphagia, cognitive deficits and mental retardation.

It is well described that the basal ganglia are responsible for proper motor coordination. The striatum (consisting of caudate nucleus and putamen) is an integral area of the basal ganglia, where glutamatergic corticostriatal neurons and dopaminergic neurons emanating from the substantia nigra make synaptic contact with medium spiny neurons (MSNs) to form circuits for proper motor control. Here, dopamine acts as a critical modulator of the corticostriatal synapse and a regulator of synaptic plasticity as medium spiny neurons harbor both glutamate and dopamine receptors (Calabresi et al., 2007; Gerfen & Surmeier, 2011; Lovinger, 2010). MSNs, expressing D1 dopamine receptor (DRD1) or D2 dopamine receptor (DRD2), then project to GABAergic neurons in the globus pallidus internal or external, respectively. These pathways are also referred to as direct or indirect pathway.

Mounting evidence demonstrated synaptic pathologies in both humans and mouse models and led to the characterization of PD as synaptopathy in the prodromal stage of the disease. Indeed, synaptic dysfunction together with an axonal dying-back mechanism have been described in association with α-synuclein (Calo et al., 2016). Various genetic mouse models without obvious motor defects, showed molecular and physiological changes of the synapse which include alterations in dopamine transmission of the nigrostriatal projections and in the functioning of the corticostriatal synapse (Calo et al., 2016; Imbriani et al., 2022; Schirinzi et al., 2016).

Whether or not PARK15 has underlying synaptopathological changes is unclear, but since the response to levodopa replacement therapy was variable in PARK15 patients, synaptic changes are likely. The studies by Fonzo et al., Shojaee et al., and Correa-Vela et al., demonstrated a positive response to treatment, while Yalcin-Cakmakli et al., reported that levodopa replacement therapy had little benefit and was accompanied with strong side effects such as dyskinesias, indicating a hypersensitivity to dopamine or was not tolerated at all (Correa-Vela et al., 2020; Di Fonzo et al., 2009; Shojaee et al., 2008; Yalcin-Cakmakli et al., 2014). Alternative treatment with dopamine receptor agonist triggered psychiatric side effects including agitation, repetitive behavior, aggression and psychotic episodes (Yalcin-Cakmakli et al., 2014). Other reports showed that the examined patients developed delusions, addictive behavior, impulse control disorder or aggression upon levodopa treatment, while two other patients showed a good response to medication but with treatment-induced dyskinesias (Lorenzo-Betancor et al., 2020; Yoo et al., 2020). Studies that performed tomographic imaging studies on PARK15 patients to determine the availability of dopamine transporter as a marker for nigrostriatal integrity, reported presynaptic defects as the amount of dopamine uptake was significantly reduced (Di Fonzo et al., 2009; Yoo et al., 2020). Neuroimaging techniques including SPECT and PET performed on PD patients in general have shown a progressive decrease in DAT (dopamine transporter), which reflects synapse malfunction or degeneration of the dopaminergic nerve endings (Bidesi et al., 2021; Eshuis et al., 2009; Hilker et al., 2005).

To understand the complexity of PARK15 syndrome, we have previously generated several mouse models and reported that systemic loss of *Fbxo7* in mice led to motor defects and premature death

during the fourth week of age (Vingill et al., 2016). To gain further insight into the role of neuronal FBXO7 in the brain, we deleted *Fbxo7* in areas relevant to PD and motor control, namely the forebrain and the substantia nigra. While the deletion in glutamatergic forebrain neurons using the NEX-*Cre* driver line resulted in strong hind limb clasping and early-onset motor dyscoordination, the deletion of *Fbxo7* in TH-positive neurons with the TH-Cre driver line led to progressive, late-onset motor dysfunctions (Vingill et al., 2016). Importantly, the latter mouse model displayed markedly reduced levels of striatal dopamine prior to the onset of motor defects (Vingill et al., 2016).

In this study, we carried out behavioral and histopathological analyses of the PARK15 mouse model, in which we deleted *Fbxo7* in glutamatergic forebrain neurons (NEX-*Cre*+/−;*Fbxo7fl/fl*, short: *Fbxo7 cKO*). We report abnormal spontaneous home cage behavior such as hyperactivity and circling, and an increase in striatal dopamine concentrations. In addition, we report alterations in the striatum in general and specific changes of the striatal synapse including increased levels of complement 1q (C1q) and the down-regulation of protein networks regulating exocytosis and endocytosis. Taken together, we have identified FBXO7 as a crucial player in the synaptic integrity of the striatum in mice which suggests that prodromal stages of parkinsonism and PARK15 syndrome are associated with major synaptic deficits.

2 | MATERIALS AND METHODS

2.1 | Antibodies used in immunohistochemistry

Mouse α-NeuN (1:1000 dilution; Millipore Cat# MAB377, RRID:AB_2298772), rabbit α-parvalbumin (1:500 dilution; Synaptic Systems Cat# 195002, RRID:AB_2156474), mouse α-GFAP (1:200 dilution; Leica Biosystems Cat# NCL-GFAP-GA5, RRID:AB_563739), rabbit α-Iba1 (1:1000 dilution; FUJIFILM Wako Shibayagi Cat# 019-19741, RRID:AB_839504), mouse α-synaptophysin (1:500 dilution; Synaptic Systems Cat# 101011, RRID:AB_887824), rabbit α-Homer1 (1:500 dilution; Synaptic Systems Cat# 160002, RRID:AB_2120990), mouse α-VGAT (1:500 dilution; Synaptic Systems Cat# 131011, RRID:AB_887872), rabbit α-VGluT1 (1:1000 dilution; Synaptic Systems Cat# 135302, RRID:AB_887877), rabbit α-tyrosine hydroxylase (1:500 dilution; Zytomed Systems Cat# 620-0336, RRID:AB_2924666), rabbit α-DAT (1:200 dilution; Millipore Cat# AB1591P, RRID:AB_90808), rabbit α-DRD1 (1:250 dilution; Synaptic Systems Cat# 376002, RRID:AB_2631217), rabbit α-DRD2 (1:500 dilution; Synaptic Systems Cat# 376203, RRID:AB_2636918), rabbit α-C1qa (1:500 dilution; Abcam Cat# ab182451, RRID:AB_2732849), rabbit α-amphiphysin (1:250 dilution; Synaptic Systems Cat# 120002, RRID:AB_887690), rabbit α-endophilin (1:100 dilution; Synaptic Systems Cat# 159002, RRID:AB_887757), mouse α-epsin1 (1:250 dilution; Santa Cruz Biotechnology Cat# sc-55 564, RRID:AB_831278), mouse α-α/β synuclein (1:250 dilution; Synaptic Systems Cat# 128011, RRID:AB_2619808), rabbit α-complexin1/2 (1:250 dilution; Synaptic Systems Cat# 122003, RRID:AB_2619793), rabbit α-YKT6 (1:50 dilution; Novus Cat# NBP1-87439, RRID:AB_11014022).

HRP-conjugated secondary antibodies, goat α-rabbit (1:1000; Dianova), goat α-mouse (1:1000; Dianova), Cy3/Alexa488-conjugated secondary antibodies were goat α-rabbit and goat α-mouse (1:1000; Dianova).

2.2 | Animal ethics statement

All experiments involving live animals have been conducted according to the animal protocol approved by LANUV (81.02.04.2021.A474, 81.02.042017.A210) and LAVES. Mice were kept in groups of 3–4 in individually ventilated cages and under specific pathogen-free conditions in the animal facility of the University Hospital RWTH Aachen, on a 12-h dark/light cycle, with food and water ad libitum.

2.3 | Transgenic mice

NEX-*Cre*+/−;*Fbxo7fl/fl* mice (referred to as *Fbxo7* cKO in results section) have been generated on a C67B/6 N background as described previously (Vingill et al., 2016). Briefly, FBXO7-deficient mice were generated by homologous recombination in C57BL/6 mouse JM8.N4 embryonic stem cells (Fbxo7tm1a(EUCOMM)Hmgu). Here, exon 4 of Fbxo7 gene was exchanged with a neomycin/lacZ cassette driven by the L1L2_Bact_P promoter. Chimeras were generated by injection of the aforementioned embryonic stem cells into C57BL/6N blastocysts. Homozygous transgene mice were then bred to 129S4/SvJaeSor-Gt(ROSA)26Sortm1(FLP1)Dym/J resulting in *Fbxo7fl/fl* knockout mouse line, which were further bred to NEX-*Cre* driver line (Goebbels et al., 2006). A total of 129 mice were used.

2.4 | Experimental design

Except from the LABORAS and HPLC analysis, which included males only. Both female and male mice were examined in the remaining analyses. The weight of the animals ranged from 18 to 23 g for younger cohorts (8 weeks) and 22–27 g for the older cohort (13 weeks). The age of the mice used in the experiment as well as the sample size are indicated in the figure legends. The experiments comprised at least one other control group (NEX-*Cre*, *Fbxo7fl/fl*, or NEX-*Cre*;*Fbxofl/fl*). Since we analyzed different genotypes, we could not use a randomization method to assign these mice into groups, but resorted to a blinding method. To blind the experiments, we have split the tasks of genotyping and the performance of experiments (behavior and HPLC analysis). For the quantitative mass spectrometry analyses, we needed a critical net weight of striatum to successfully run the sucrose gradient.

Hence, we calculated how many mice we needed to have the required brain mass. The collaborative party was handed over the purified synaptosomes not knowing which sample belonged to which group. For immunohistochemistry, we used G-power to calculate the number of animals to support our findings with an independent analysis. The brain sections were blinded, then subjected to immunohistochemical analyses and quantification, prior to unblinding. The experiments comprised different outcome measures, which are indicated in the figure legends. All animals sacrificed for the experiments were included in the analyses. Animal suffering caused by genetic mutations was reduced due to limitation of life span to 13 weeks prior to analyses. During this period of time, control and cKO mice cannot be distinguished in the cage. The suffering of the mice prior to the analyses is limited to one-time injection of anesthetics or rapid cervical dislocation.

2.5 | Laboratory animal behavior observation, registration and Analysis system (LABORAS)

The LABORAS home cage behavioral monitoring system (Metris b.v., Hoofddorp, The Netherlands) harbors a mechanosensitive platform that is mounted on two force transducers, attached to an underlying plate (Dere et al., 2014; El-Kordi et al., 2013). Mouse home cages were placed on the sensor platform, with the grid suspended above. Vibrations of different frequencies and amplitudes caused by specific animal movements were transformed into electrical signals and digitized. These signals were then translated into specific behavioral categories and the dominating behavior at the time was quantified by the LABORAS software. Time spent performing a behavior and its frequency were quantified. Animals (male mice NEX-*Cre* ($n=5$), *Fbxo7fl/fl* ($n=5$) or NEX-*Cre*;*Fbxo7fl/fl* ($n=6$)) were acclimatized to the system for 1 h, and recordings were conducted for 15 h during the dark cycle.

2.6 | Open field

Open field analysis was conducted in a circular open field (60 cm diameter). The exploratory behavior of the mouse was recorded using an automatized tracking-software (Viewer2, Biobserve, Germany). The track of the animals' ambulatory behavior has been recorded continuously using x,y coordinates and locomotor patterns indicative for thigmotaxis behavior or excessive circling behavior have been determined by visual inspection of the total open field area covered and by determining clusters respectively "hot zones" with repeated crossings of movement tracks that are indicative of excessive circling behavior. Animals (11 male mice NEX-*Cre*, 14 *Fbxo7fl/fl* ($n=14$) or 15 NEX-*Cre*;*Fbxo7fl/fl*) were acclimatized to the behavior room for 1 h, and recordings were conducted for 7 min during the light cycle.

2.7 | Neurochemical analysis of dopamine and metabolites

HPLC analysis was conducted as previously described (Tonges et al., 2012). Male mice NEX-*Cre* ($n=5$), *Fbxo7fl/fl* ($n=6$) and NEX-*Cre*;*Fbxo7fl/fl* ($n=10$) were sacrificed via cervical dislocation and striata were immediately dissected on ice. Striatal tissue of each mouse was homogenized separately in a bead mill homogenizer (Precellys 24®, Peqlab, Erlangen, Germany) with 50 µL of 0.1 M perchloric acid per mg of tissue. Samples were subjected to centrifugation (13.4 g, 5 min), supernatant transferred to a clean tube and subjected to further centrifugation (13.4 g, 10 min, 4°C). 20 µL of supernatant was injected onto a C18 reverse-phase HR-80 catecholamine column (ESA). Dopamine, 3,4-dihydroxyphenylacetic acid (DOPAC), and homovanillic acid (HVA) levels were quantified by HPLC with electrochemical detection. The mobile phase (pH = 4.3) consisted of 6.9 g/L sodium acetate, 48 mg/L EDTA, 7.3 g/L citric acid, 105 mg/L octane sulfonic acid, and 10% methanol. Flow rate was 0.4 mL/min. Peaks were detected by an ESA Coulochem III with a model 5010 detector (E1 = 50 mV, E2 = 400 mV). Data were collected and processed using the Chromeleon computer system (DioNEX, Idstein, Germany).

2.8 | Transcardial perfusion

To perfuse a mouse, the animal was weighed and anesthetized by intraperitoneal injection with 10 µL/g of Ketamine/Xylazine solution, a standard anesthetic used prior to perfusion. Thereafter, the mouse was tested for the absence of reflexes or twitching. The mouse was mounted onto a styrofoam surface and an incision through the skin and abdominal wall beneath the rib cage was made to expose the heart. Another incision in the diaphragm and a continuous cut along the rib cage were made to expose the pleural cavity. Finally, lateral cuts up to the collar bone were made and the rib cage was lifted and fixed with needle. The connective tissue around the heart was carefully trimmed, prior to insertion of the 27G butterfly cannula into the left ventricle of the heart and fixation with a bulldog clamp. The peristaltic pump was switched on and a small incision in the right atrium was made. The mouse was perfused with approx. 10 mL of PBS (5 weeks of age) or 15–20 mL of PBS (13 weeks of age). The peristaltic pump was stopped and switched to *4%* PFA for perfusion. Again, the mouse was perfused with approx. 10 mL or 15-20 mL of 4% PFA for 5-week or 13-week-old mice. The transcardial perfusion was successful when the mouse was stiff and inner organs, e.g. the liver, were pale and spongy to the touch. The brains were dissected for further processing. Both male and female mice NEX-*Cre*,*Fbxo7fl/+* ($n=6$) or NEX-*Cre*;*Fbxo7fl/fl* ($n=6$), age 5 weeks and 13 weeks were included in the striatum analysis, and *Fbxo7fl/fl* ($n=3$) or NEX-*Cre*;*Fbxo7fl/fl* ($n=3$), age 12 weeks, for the cortical analysis.

2.9 | Immunohistochemistry

Isolated brains from perfused mice were postfixed in 4% PFA over night at 4°C, washed once in PBS and then incubated in a 30% sucrose solution over night at 4°C. Brains were then embedded in OCT: 30% sucrose/PBS (1:2) and stored at −80°C. 30 μm sections of the striatum and cortex were cut on a Cryostat and stored in PBS/0.04%NaN_3 at 4°C. Three coronal sections from each brain were incubated in blocking buffer for 30 min (10% goat serum, 3% BSA, 0.3% Triton X100 in PBS) before adding primary antibody in blocking buffer for 24 or 48 h. Fluorophore-conjugated secondary antibody and the nuclear dye DAPI (1:8000) were applied for 1 h at RT. Sections were mounted on poly-lysine slides (Thermo Scientific) with Moviol mounting medium.

Images were obtained using the Carl Zeiss confocal microscope with the Andor DU-88 Camera and a 20× (NeuN, PV, GFAP and Iba1) or a 63× (others) objective. Customized macros designed by Ippolito & Eroglu (Ippolito & Eroglu, 2010) were used to analyze and quantify fluorescence images. The threshold was specifically set in each macro to separate and to count the number of immunostaining-positive neurons, the percentage of glial cell- positive area or the number of immunostaining-positive puncta. Four striatal areas and two cortical areas for each hemisphere were quantified per section. According to previous experiments analyzing synptophysin (puncta/10000 μm^2), we calculated (G*power) with the following parameters to determine sample size (7 mice per group). Effect size: min1.0, actual power: 0.833. $p < 0.05$. Control mice (mean: 975, var: 16786, StdDev: 129), cKO mice (mean: 1197, var: 27963, StdDev: 167).

2.10 | Purification of synaptic membranes

Striata from 22 NEX-*Cre*,*Fbxo7fl*/+ and 22 NEX-*Cre*,*Fbxo7fl*/fl mice (with equal numbers of males and females in each group, 8 weeks), killed via cervical dislocation, were isolated and homogenized with 3 mL solution A (0.32 M sucrose, 1 mM NaHCO3) using a Dounce homogenizer and a glass pestle. Homogenization was performed by pressing down and lifting the pestle 30 times, resulting in the lysate (homogenate H). The homogenate was applied to a discontinuous sucrose density gradient consisting of 0.85, 1.0 or 1.2 M sucrose. After centrifugation at 82 500 g for 2 h at 4°C, the interphase between 1.0–1.2 M sucrose was harvested and resuspended with solution A, then centrifuged at 100 000 *g* for 20 min. 500 μL were set aside as soluble (S) fraction. The pellet was resuspended in 2.5 mL of 6 mM Tris-Cl, pH 8 using 21G and 27G needles and incubated for 45 min at 4°C to obtain the synaptosome fraction (SF). Then, 2 mL of P2C was centrifuged at 32 800 g for 20 min to separate the synaptic membrane from the synaptosomes. The supernatant was harvested as synaptic cytoplasm and coarse synaptic vesicles (SC/CSV) fraction, and the pellet was harvested as coarse synaptic membrane (CSM) fraction. Subsequently, the CSM fraction was applied to a second discontinuous sucrose density gradient with 0.85 M, 1.0 or 1.2 M sucrose. After centrifugation at 82 500 *g* for 2 h at 4°C, the interphase between 1.0 and 1.2 M sucrose was harvested and resuspended with solution A, then centrifuge 100 000 g for 20 min, and 500 μL was set aside as soluble fraction (S2). The pellet was resuspended in 0.5 mL of 6 mM Tris-Cl, pH 8 using 21G and 27G needles to obtain the purified synaptic membrane (SM) fraction. The purified fractions were run on a 4–12% gradient SDS-PAGE gel and subjected to Coomassie Brilliant Blue G-250 staining prior to quantitative mass spectrometry analyses.

2.11 | Immunoblot analysis

Mouse tissue was lysed in TX100 buffer (150 mM NaCl, 50 mM Tris–HCl pH 7.5, 1 mM EDTA, 1% Triton X100, protease inhibitors), samples were run on a 4–12% SDS-PAGE gel and proteins were transferred to a nitrocellulose membrane (Amersham). The membrane was blocked for 30 min using 4% milk powder in PBS/Tween20. Primary antibody was diluted in 3% bovine serum albumin applied over night at 4°C or for 1 h at room temperature (RT). Membranes were subjected to secondary HRP-conjugated antibodies diluted in 4% milk powder in PBS/Tween20 for 45 min at RT. Protein bands were detected by enhanced chemiluminescence (Thermo Scientific) using camera operating by ALLIANCE.

2.12 | Quantitative mass spectrometry analyses

Synaptosomes from 22 NEX-*Cre*,*Fbxo7fl*/+ (control) and 22 NEX-*Cre*,*Fbxo7fl*/fl (cKO) mice (equal numbers of males and females) were separated into three biological replicates, which were separated on SDS-gels and stained with Coomassie Brilliant Blue. Five bands per gel lane (resulting in 30 samples) were excised and proteolytically digested "in-gel" with trypsin as described previously (von Kriegsheim et al., 2008). The resulting tryptic peptides were desalted using homemade C18 columns, lyophilized, resuspended in 10% formic acid and analyzed by liquid chromatography-coupled mass spectrometry. Peptides were initially trapped on a precolumn (Acclaim PepMap100, C18, 5 μm, 100 Å, 300-μm inner diameter ×5 mm, Thermo Scientific) in Buffer A (0.1% formic acid in water) for 10 min. Subsequently, the samples were separated on an analytical column (Easyspray E802, 25 cm length, 40°C column oven temperature, 2 kV; Thermo Scientific) using a 140-min gradient (0–10 min, 5% buffer B (80% acetonitrile, 0.1% formic acid); 10–104 min, 5–35% buffer B; 104–114 min, 35–45% buffer B; 114–119 min, 99% buffer B; 119–120 min, 95–5% buffer B; 120–140 min, 5% buffer B) at 300 nL/min and injected into the mass spectrometer. The peptides were then analyzed on an Q Exactive Plus instrument (Thermo Scientific) in data-dependent mode. A top20 method was used, with a full scan mass range of 350–1600 and 70 k resolution. Fragmentation was carried out at 17500 resolution an isolation window of 1.8 *m/z* and a collision energy of 27%.

The resulting raw data files were analyzed using the MaxQuant software suite (version 1.6.10.43; Tyanova et al., 2016) with the label-free quantification algorithm and the built-in Andromeda search engine. The resulting spectra were searched against the mouse UniProt database version 02/2019.with default mass tolerance settings. Trypsin was set as the protease (with two missed cleavages allowed). Fixed modification: carbamidomethylation (Cys); variable modifications: oxidation (Met), and N-terminal protein acetylation. False discovery rate (FDR) was kept at the default settings (0.01 for both peptides and proteins); minimum peptide length: seven amino acids.

The resulting MaxQuant file "proteinGroups.txt" was then analyzed and filtered using Perseus (version 1.6.14.0 (PMID: 27348712)). The protein entry list was filtered for entries corresponding to "reverse", "only identified by site" and "potential contaminants", which were all removed. To be considered for further evaluation, a protein had to be identified (a) with at least two unique peptides and (b) in all samples of at least one condition. Value imputation based on normal distribution was performed after the last filtering step using the default values in Perseus. Finally, a *t*-test was performed and results were plotted in a volcano-type graph with the X-axis displaying $\log_2$ fold change and thresholds at −0.5 and 0.5; and the Y-axis displaying log10 *p*-value and threshold at $p < 0.05$. The mass proteomics data have been deposited to the ProteomeXchange Consortium (Deutsch et al., 2023) via the PRIDE (Perez-Riverol et al., 2022) partner repository with the dataset identifier PXD044119. Project DOI: 10.1111/jnc15962.

2.13 | Statistical analyses

GraphPad PRISM 9 was used to perform all statistical analyses using one-way ANOVA followed by Bonferroni-corrected multiple comparison post-hoc test or the Student's *t*-test for independent samples (=two-tailed, unpaired). Shapiro–Wilk test revealed normal distribution for LABORAS in Figure 1 and HPLC in Figure 2 data. Normal and lognormal distribution was verified using Shapiro–Wilk test or D'Agostino & Pearson test for immunohistochemistry analyses. The sample size of each group is depicted as dots in the individual bar graphs of each figure. Degrees of freedom, *F*-values, *t*-values and *p*-values are shown in Tables S1–S3. Reported *p*-values are always two-tailed and considered significant if $p < 0.5$.

3 | RESULTS

FBXO7 is crucial for proper neuronal functioning. Transgenic mice, in which we deleted *Fbxo7* in glutamatergic neurons of the forebrain (NEX-*Cre*;*Fbxo7 fl/fl*, short: *Fbxo7* cKO), displayed hind limb clasping not only severe early-onset motor coordination defects on the rotarod and balance beam (Vingill et al., 2016). Despite the mice's motor defects, we observed that they were hyperactive. This observation prompted us to delve into further examinations including behavioral tests, HPLC, immunohistochemistry and quantitative mass spectrometry analyses (Table 1).

To examine whether or not the hyperactivity was due to a novel environment, we used the LABORAS (Laboratory Animal Behavior Observation Analysis System) system to monitor spontaneous behavior of mice in their home cage over a period of 15 h. We found that the distance traveled and the running speed of *Fbxo7* cKO mice was significantly higher as compared to the control groups (NEX-*Cre* and *Fbxo7fl/fl*), (Figure 1a,b; Table S1). *Fbxo7* cKO mice were also more active at any given time, that is during the light (inactive) and dark (active) periods of the day (Figure 1c; Table S1), and were consequently less immobile (Figure 1d; Table S1).

Strikingly, *Fbxo7* cKO mice showed excessive circling behavior during the short-term examination in the open field arena, which we did not observe in any of the control groups (Figure 1e; Table S1). The analysis of the time spent in the periphery, intermediate zone and center of the open field arena also revealed differences as *Fbxo7* cKO mice tended to spend less time in the periphery and more time in the intermediate zone and center than control groups, indicating a difference in thigmotactic behavior (Figure 1f; Table S1). LABORAS conclusively confirmed the presence of behavioral stereotypies as *Fbxo7* cKO mice showed excessive circling behavior during the 15h surveillance (Figure 1g; Table S1). There was no within-group preference for clockwise/counter-clockwise circling (Figure 1h; Table S1) that would be indicative of a lateralized neuropathology. While *Fbxo7* cKO mice showed no difference in grooming behavior (Figure 1i; Table S1), they displayed other behavioral abnormalities such as enhanced rearing (Figure 1j; Table S1) and scratching (Figure 1k; Table S1). These results indicate that loss of *Fbxo7* in glutamatergic neurons of the forebrain triggers hyperactivity and stereotypic behavior.

Since the loss of *Fbxo7* in TH+ neurons led to a decrease in striatal dopamine concentrations (Vingill et al., 2016), we wondered whether or not loss of *Fbxo7* in glutamatergic forebrain neurons had any effect on dopamine levels in the striatum as well. Using HPLC analysis, we found a significant increase in *Fbxo7* cKO mice as compared to control groups (Figure 2a; Table S2), while we found no changes in its metabolites DOPAC (3,4-Dyhydroxyphenylacetic acid) and HVA (Homovanillic acid) (Figure 2b,c; Table S2), but a significant change in the metabolite ratio (Figure 2d; Table S3).

We have previously shown that there was no significant increase in TUNEL+ cells in the cortex of *Fbxo7* cKO mice (Vingill et al., 2016), which was consistent with only marginal changes in the number of NeuN+ neurons in the cortex of 12-week-old mice (Figure 3a; Table S3), confirming that deletion of *Fbxo7* in the glutamatergic forebrain neurons (including corticostriatal neurons) did not lead to noticeable cell death. Hence, we raised the question of how loss of *Fbxo7* in corticostriatal neurons together with the increase in striatal dopamine affected the structural and synaptic integrity of the striatum. We focused on the examination of the striatum (putamen) and additionally the globus pallidus internal and external, the output regions of the MSNs (Figure 3b). We carried out immunohistochemical

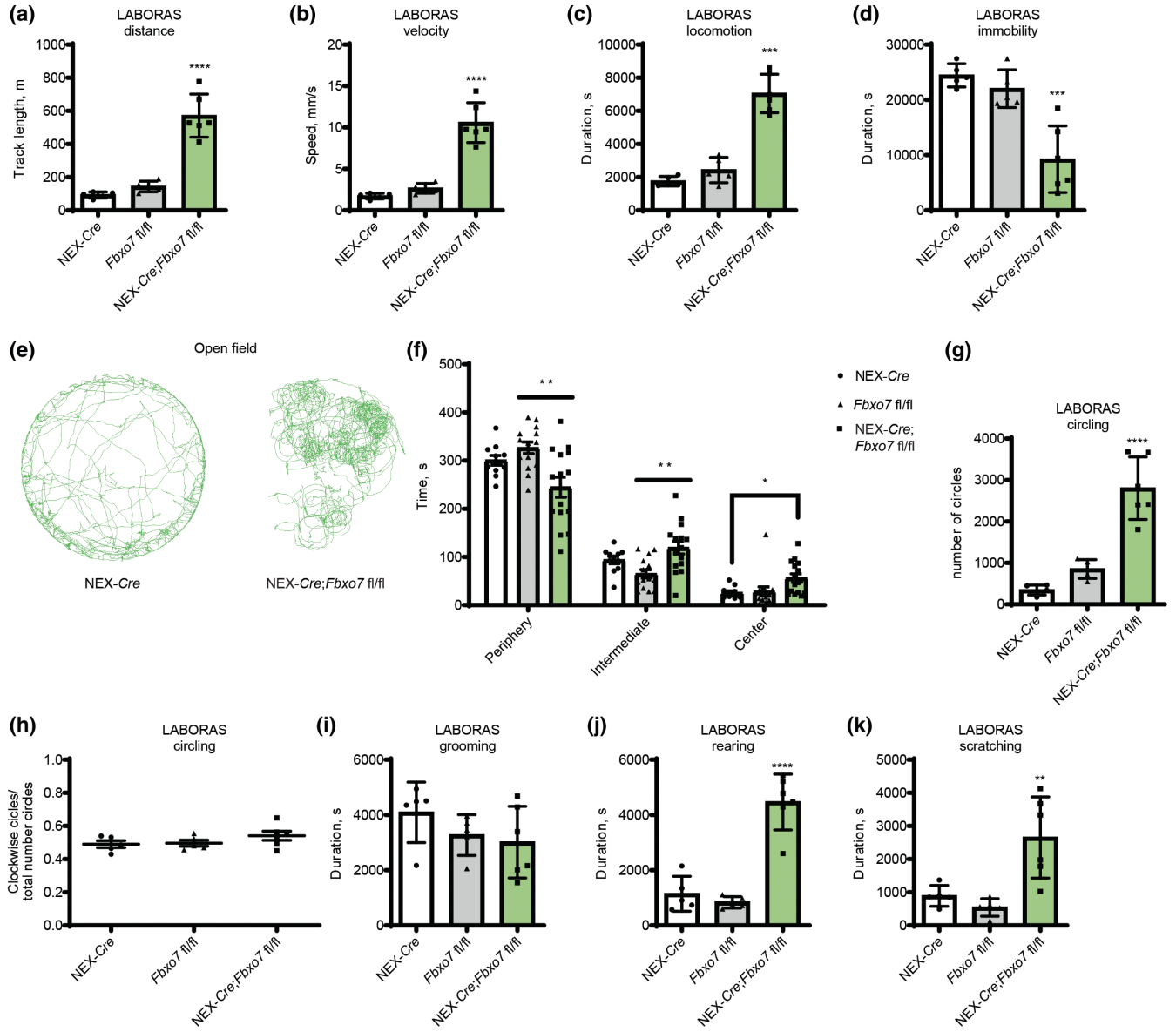

FIGURE 1 Deletion of *Fbxo7* in the forebrain causes hyperactivity and stereotypic behavior. (a–d) 8-week-old, male NEX-*Cre* ($n=5$), *Fbxo7fl/fl* ($n=5$) or NEX-*Cre*;*Fbxo7fl/fl* ($n=6$) mice were analyzed with in the LABORAS system for 15 h. Distance traveled (a), average velocity (b) locomotion duration (c), time spent immobile (d) were assessed. One-way ANOVA (Bonferroni), $^{**}p<0.01$, $^{***}p<0.001$, mean ± SEM. (e) Representative tracks of movement of NEX-*Cre* and circling pattern of NEX-*Cre*;*Fbxo7fl/fl* mice in open field arena. (f) 8-week-old, male NEX-*Cre* ($n=11$), *Fbxo7fl/fl* ($n=14$) or NEX-*Cre*;*Fbxo7fl/fl* ($n=15$) mice were analyzed with in the Open Field arena for 7 min. Time spent in periphery, intermediate zone and center were assessed. Two-way ANOVA (Bonferroni), $p<0.05$, $^{**}p<0.01$, mean ± SEM. (g–k) Quantification of circling (g) and circling direction (h), grooming (i) rearing (j) and scratching (k) behavior of 8-week-old, male NEX-*Cre* ($n=5$), *Fbxo7fl/fl* ($n=5$) or NEX-*Cre*;*Fbxo7fl/fl* ($n=6$) from LABORAS system. One-way ANOVA (Bonferroni), $^{**}p<0.01$, $^{***}p<0.001$, mean ± SEM.

analyses at adolescent age (5 weeks) and at a young adult stage (13 weeks) to uncover alterations and to monitor the dynamics of the changes. In the analyses, we refer simply to globus pallidus as the confocal imaging following the immunohistochemistry made it difficult to discern the external and the internal regions. In addition, owing to a progressive deterioration of *Fbxo7* cKO mice beyond 13–14 weeks of age and to ensure animal welfare, we refrained from assessing older mice with more severe neurological symptoms.

The analyses showed no significant loss of NeuN+ neurons or PV (parvalbumin) + interneurons in *Fbxo7* cKO mice compared to control NEX-*Cre*;*Fbxo7fl/+* littermates in any of the analyzed regions or at any age (Figure 3c,d; Table S3). However, we observed an increase in GFAP+ and Iba1+ areas in *Fbxo7* cKO mice in both globus pallidus and the putamen at all ages (Figure 3e,f; Table S3). These results indicate that while there was little or no cell death, inflammatory processes (astrogliosis and microgliosis) were triggered as a result of FBXO7 loss. These results also suggest that the neuropathology is still at an early stage.

PD is a neurodegenerative disorder but also a synaptopathy, which prompted us to analyze synaptic marker proteins to establish

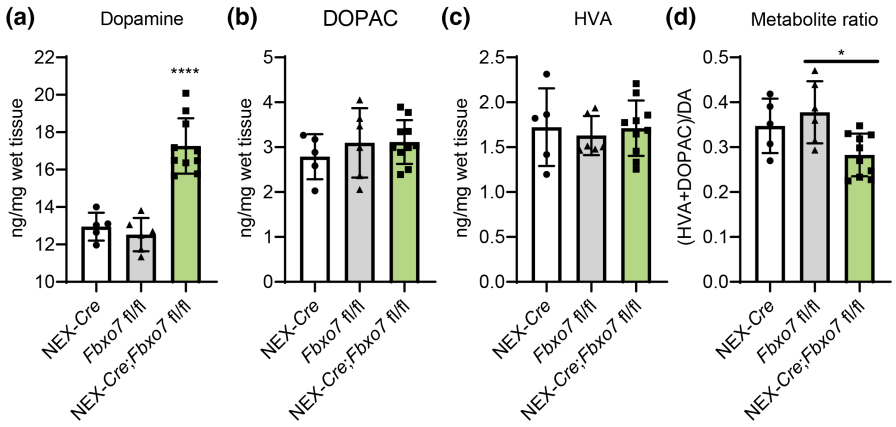

FIGURE 2 NEX-*Cre*; *Fbxo7fl/fl* mice show an increase in dopamine in the striatum. (a–d) Striatal tissues from 8-week-old NEX-*Cre* ($n=5$), *Fbxo7fl/fl* ($n=6$) and NEX-*Cre*;*Fbxo7fl/fl* ($n=10$) were subjected separately to HPLC analysis for dopamine (a), DOPAC (b) and HVA (c). Metabolism is shown as ratio of HVA and DOPAC to dopamine (d). One-way ANOVA (Bonferroni), $^{*}p<0.05$, $^{***}p<0.001$, mean ± SEM.

TABLE 1 "Experimental design of the study"

Method	Age of mice	Number and biological sex of mice
1. LABORAS	8 weeks	16 males
2. HPLC of striata	8 weeks	21 males
3. General Immunohistochemistry	5 and 13 weeks	Total of 24, 17 males and 7 females
4. Quantitative mass spectrometry (qMS)	8 weeks	Total of 44, equal numbers of males and females
4a. Immunohistochemistry to validate qMS	5 and 13 weeks	Same 24 mice that were analyzed in 3

whether or not there is a change in the number of synapses as there is little or no cell death in the striatum. The quantification however showed no change in the presynaptic marker protein synaptophysin or the postsynaptic marker protein homer1 (Figure 4a,b, Table S3). We also quantified the colocalization of synaptophysin and homer1 as a measure of synapse number and found no change in the narrow time window, in which the cKO mice can be analyzed before their condition is starting to deteriorate (Figure 4c, Table S3). We also examined both VGluT1 and VGAT, vesicular transport proteins required to load glutamate and GABA into vesicles, respectively. Here, we detected no change in VGluT1 in globus pallidus but a significant decrease in *Fbxo7* cKO mice in the putamen at both ages (Figure 4d, Table S3). In contrast, VGAT was significantly increased in the globus pallidus at both ages without any change in the putamen (Figure 4e, Table S3). Of note, PV+ neurons are GABAergic interneurons, whose number did not change. These findings suggest a differential effect on the glutamatergic and GABAergic transmitter system in *Fbxo7* cKO mice.

Since striatal dopamine levels were increased, we raised the question as to how the dopamine transporter and dopamine receptors were affected. We first assessed the levels of TH, the rate-limiting enzyme in dopamine synthesis expressed by nigrostriatal neurons and found that there was an increase in older *Fbxo7* cKO mice both in the globus pallidus and putamen (Figure 5a; Table S3). Interestingly, we also observed that DAT (dopamine transporter) was significantly up-regulated in the areas of interest at both ages (Figure 5b, Table S1). While we found little or no change of D1 dopamine receptor (DRD1) (Figure 5c, Table S3), D2 dopamine receptor (DRD2) was up-regulated in the brain regions examined at all ages and all regions (Figure 5d, Table S3). Taken together, loss of FBXO7 not only affects striatal dopamine levels but also proteins of the dopaminergic pathway.

Next, we decided to take a closer look at the protein composition of the striatal synapse using a quantitative mass spectrometry approach. In a proof-of-principle experiment, we performed sucrose density gradient centrifugation to purify synaptic membranes from brain followed by quantitative mass spectrometry (qMS) and gene ontology analyses to ensure the enrichment of proteins characteristic for their synaptic localization. We carried out gene ontology of the identified proteins and found that a large percentage of proteins were allocated to synaptic function-related groups (Figure S6).

Encouraged by these results, we isolated striata from male and female *Fbxo7* cKO and control mice (NEX-*Cre*;*Fbxo7fl/+*) at 8 weeks of age and purified synaptic membranes from the striatum, followed by qMS. We verified the presence of the presynaptic marker VGluT1 and the postsynaptic marker PSD95 in the synaptic membrane fraction using immunoblotting (Figure 6a). The quantitative comparison of the identified proteins from *Fbxo7* cKO and control mice revealed changes but also a large number of proteins that did not show any difference (mass spectrometry data have been deposited to ProteomeXchange consortium; Table S4). The major changes that fit the criteria of the qMS analysis are depicted in a volcano plot (Figure 6b). We next carried out STRING analyses (string-db.org) of up-regulated and down-regulated proteins in *Fbxo7* cKO mice to identify protein networks as it provides reliable clues about biological processes affected by FBXO7 loss and hence its functional implications. We examined the top 60 up-regulated proteins ($\log_2(FC)>0.9$) with STRING and found several networks. Here, we identified C1qb and c among the proteins that displayed

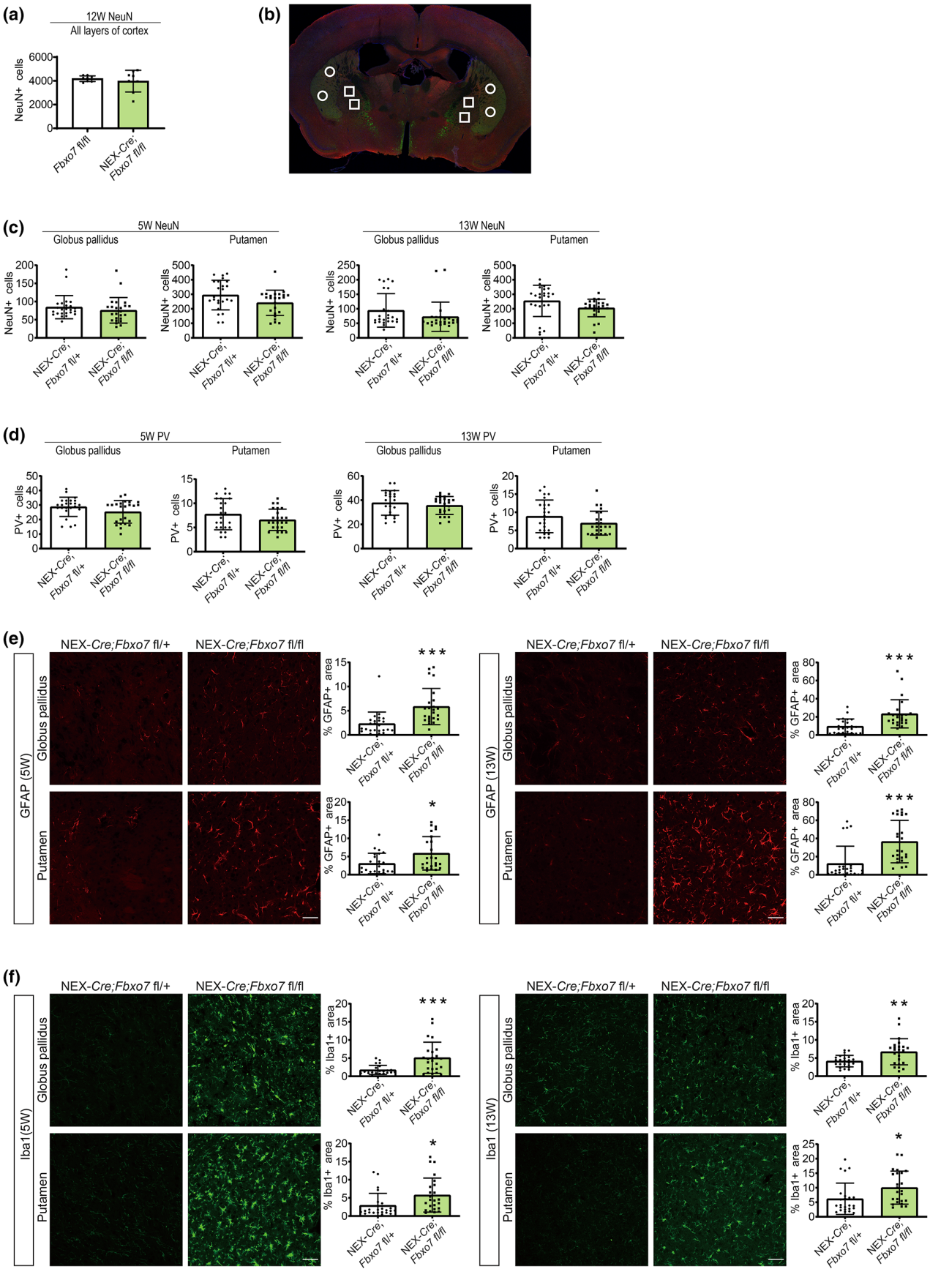

FIGURE 3 No loss of neurons but astrogliosis and microgliosis in the striatum. (a) Coronal cryosections of 12-week-old *Fbxo7fl/fl* (3 mice per age group) or NEX-*Cre*;*Fbxo7fl/fl* (6 mice per age group) forebrains were subjected to immunostaining with the NeuN antibody. NeuN+ neurons in the cortex were included in the analysis using an ImageJ-based macro. Dots per graph represent the sum of non-overlapping images of a section (cortex) per mouse. Student's *t*-test (mean ± SEM). (b) Sagittal view of representative brain section used in analyses. Circles and squares indicate the regions within the striatum and the globus pallidus, respectively, where the immunopositive puncta or areas were counted. (c, d) Coronal cryosections of 5- and 13-week-old NEX-*Cre*,*Fbxo7fl/+* (6 mice per age group) or NEX-*Cre*;*Fbxo7fl/fl* (6 mice per age group) forebrains that were subjected to immunostaining with the NeuN (b) or PV (c) antibody, respectively. NeuN+ or PV+ neurons in the putamen or globus pallidus per animal were included in the analysis. 24 dots per graph represent the sum of 4 non-overlapping images of a section (of putamen or globus pallidus) per mouse. Student's *t*-test (mean ± SEM). (e, f) Representative images of coronal cryosections of 5- and 13-week-old NEX-*Cre*, *Fbxo7fl/+* (6 mice per age group) or NEX-*Cre*;*Fbxo7fl/fl* (6 mice per age group) forebrains that were subjected to immunostaining with the GFAP (d) or Iba1 (e) antibody, respectively. GFPA+ or Iba1+ cells in the putamen or globus pallidus per animal were included in the analysis. 24 dots per graph represent the sum of 4 non-overlapping images of a section (of putamen or globus pallidus) per mouse. Student's *t*-test (*$p < 0.05$, **$p < 0.01$, ***$p < 0.001$, mean ± SEM). Magnification 20×, scale bar = 50 μm.

the largest change (Figure 6c). Interestingly, C1b and c are components of a multi-protein complex involved in synaptic pruning (Stevens et al., 2007).

With immunohistochemical analyses, we validated the changes revealed by qMS and examined the expression and dynamics of the candidates in 5- and 13-week-old mice. We found that C1q was significantly up-regulated in the putamen and also in the globus pallidus at both ages (Figure 7a; Table S3). Owing to the role in synaptic pruning, we analyzed the colocalization of C1q and synaptophysin. While there was no localization in the control group, we observed a significant colocalization in the *Fbxo7* cKO mice in the putamen of 13-week-old mice (Figure 7b, Table S3). These results indicate that the up-regulation of C1q is associated with an increase in synaptic localization of this protein at a more progressive stage of the disease.

Among the down-regulated proteins (log2FC < −0.5), we analyzed 200 proteins using STRING and several networks appeared. Strikingly more than 15% of these proteins were associated with endocytosis or exocytosis. For our analyses, we singled out functionally and biochemically related proteins that were at the core of the network and which we sought to validate with immunohistochemical analyses (Figure 8a,b).

We selected proteins of the exocytosis network and examined α-synuclein, which is involved in SNARE complex assembly and whose mutations have been are causative for an autosomal-dominant variant of Parkinson disease (Burré et al., 2010; Polymeropoulos et al., 1997). We found a significant reduction in both regions at both ages (Figure 9a; Table S3). Furthermore, we included YKT6, which was originally described as a SNARE protein (McNew et al., 1997). YKT6 displayed a significant decrease in the globus pallidus at 5 weeks of age, but merely a downward trend at 13 weeks of age, while YKT6 levels in the putamen were significantly reduced at both ages (Figure 9b; Table S3). To test the idea that SNARE-mediated exocytosis was impaired, we examined complexin1/2, a regulator of a late step in exocytosis (Reim et al., 2001). While this protein had been included in previous analyses of the qMS data, state-of-the-art stringency of the analysis left it just below the cut-off. Our histological analyses however painted a clear picture of complexin1/2 down-regulation and revealed a significant decrease in the globus pallidus of *Fbxo7* cKO mice at 5 and 13 weeks of age. The putamen showed a significant decrease at 5 weeks and a downward trend at 13 weeks of age (Figure 9c; Table S3).

Finally, we aimed at validating the down-regulated protein network involved in endocytosis. We examined the levels of amphiphysin, which has been described in clathrin-mediated endocytosis (Takei et al., 1999), and found a robust down-regulation in globus pallidus and putamen in both 5- and 13-week-old *Fbxo7* cKO mice (Figure 10a; Table S3). Endophilin A1, originally described as essential for the formation of synaptic vesicles (Schmidt et al., 1999), showed the same significant down-regulation in the globus pallidus at both ages. In the putamen however an initial downward trend at 5 weeks of age developed into a significant effect at 13 weeks of age (Figure 10b; Table S3). For epsin-1, a core component of the endocytic clathrin machinery (Hawryluk et al., 2006), we observed a significant down-regulation in both brain regions at both ages (Figure 10c; Table S3). Collectively, our results support the view that FBXO7 plays a crucial role in endocytosis and exocytosis protein networks at the striatal synapse of glutamatergic projections neurons.

4 | DISCUSSION

In this study, we have dissected the functional contribution of FBXO7 in glutamatergic projections neurons of the forebrain in parkinsonism using a mouse model in which *Fbxo7* was deleted using the NEX-*Cre* driver line. We then investigated the behavioral effects of the *Fbxo7* cKO mice and observed hyperactivity and stereotypies together with an increase in striatal dopamine levels. Upon examination of the striatum as integral area of corticostriatal and nigrostriatal projections, we found astro- and microgliosis as well as changes in the glutamatergic, GABAergic and dopaminergic pathway. Quantitative analysis of striatal synaptic material revealed significant up-regulation of complement 1q and the down-regulation of endocytosis and exocytosis networks.

While we have previously reported motor dysfunctions in the *Fbxo7* cKO mice that comprise hind limp clasping and deficits in motor coordination (Vingill et al., 2016), analysis of home cage behavior revealed excessive activity and circling behavior. Hyperactivity has also been found in *DAT−/−* mice, which displayed increased extracellular levels of dopamine (Gainetdinov

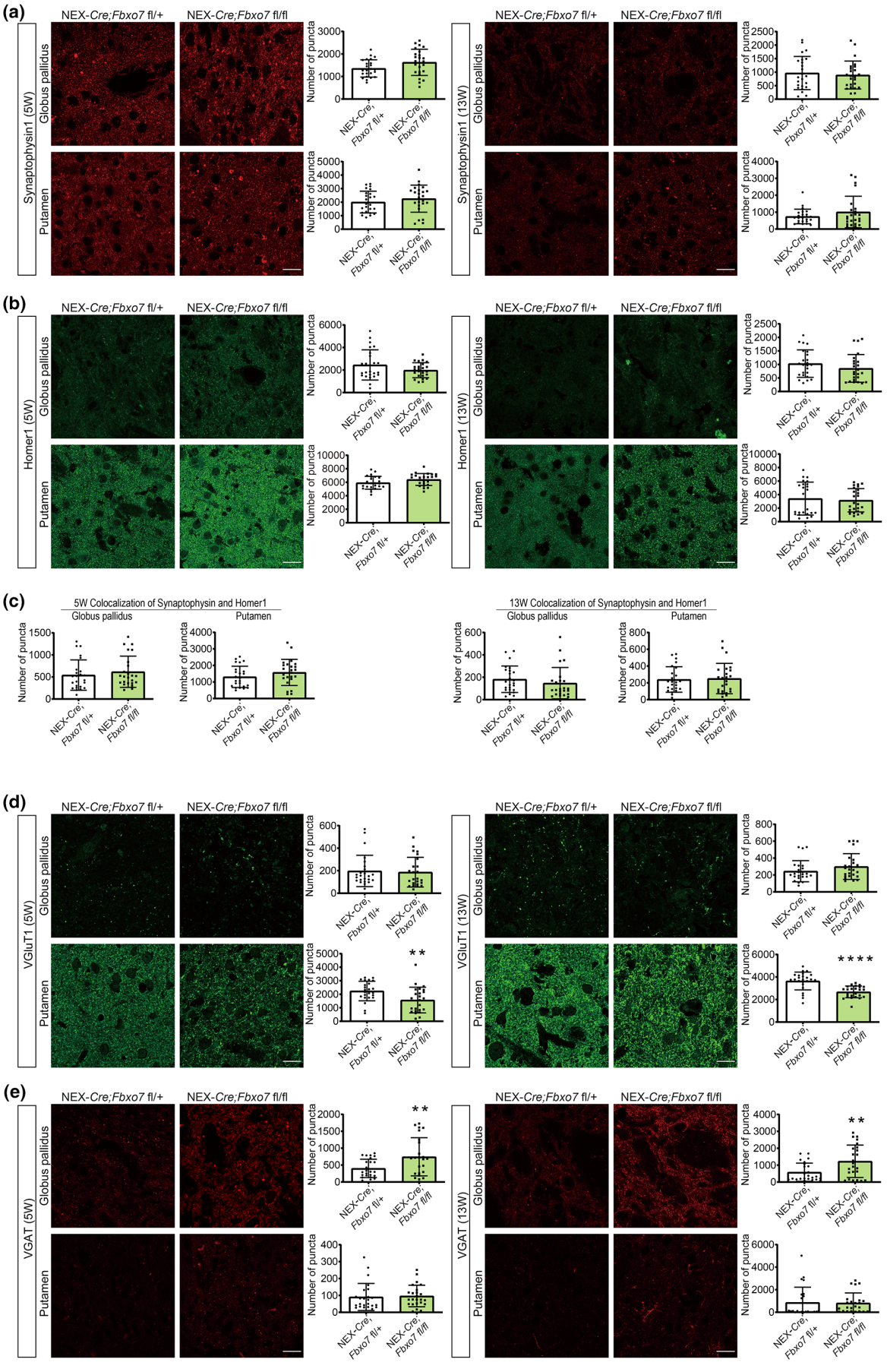

FIGURE 4 No change in synapse number upon loss of Fbxo7 but changes in glutamatergic and GABAergic pathways. (a, b) Representative images of coronal cryosections of 5- and 13-week-old NEX-*Cre*,*Fbxo7fl*/+ (6 mice per age group) or NEX-*Cre*;*Fbxo7fl/fl* (6 mice per age group) forebrains that were subjected to immunostaining with the synaptophysin (a) or homer1 (b) antibody, respectively. Synaptophysin + or homer1+ puncta in the putamen or globus pallidus per animal were included in the analysis using an ImageJ-based macro. 24 dots per graph represent the sum of 4 non-overlapping images of a section (of putamen or globus pallidus) per mouse. Student's *t*-test (mean ± SEM). Magnification 63x, scale bar = 20 μm. (c) ImageJ-based macro was used to quantify the number of co-localized synaptophysin+ and homer1+ puncta of 5- and 13-week-old NEX-*Cre*,*Fbxo7fl*/+ (6 mice per age group) or NEX-*Cre*;*Fbxo7fl/fl* (6 mice per age group) mice. 24 dots per graph represent the sum of 4 non-overlapping images of a section (of putamen or globus pallidus) per mouse. Statistical analysis was performed using Student's *t*-test (mean ± SEM). (d, e) Representative images of coronal cryosections of 5- and 13-week-old NEX-*Cre*,*Fbxo7fl*/+ (6 mice per age group) or NEX-*Cre*;*Fbxo7fl/fl* (6 mice per age group) forebrains that were subjected to immunostaining with the VGluT1 (d) or VGAT (e) antibody, respectively. VGluT1+ or VGAT+ puncta in the putamen or globus pallidus per animal were included in the analysis using an ImageJ-based macro. 24 dots per graph represent the sum of 4 non-overlapping images of a section (of putamen or globus pallidus) per mouse. Student's *t*-test (**$p < 0.01$, ****$p < 0.0001$, mean ± SEM). Magnification 63×, scale bar = 20 μm.

et al., 1998; Giros et al., 1996). *DAT*−/− rats underscored the effects of elevated dopamine as animals displayed hyperactivity and circling (Cinque et al., 2018; Leo et al., 2018). Hyperactivity is also reminiscent of a mouse model overexpressing DRD2 (Kramer et al., 2011). Furthermore, circling behavior and hyperlocomotion are phenotypes that were observed in rats that have undergone unilateral lesions of the substantia nigra followed by dopamine agonist (apomorphine) or levodopa treatment (Glick et al., 1974; Ungerstedt & Arbuthnott, 1970). Repetitive behavior was also reported in a PARK15 patient in response to dopamine agonist treatment (Yalcin-Cakmakli et al., 2014). In general, approximately 10% of the levodopa-treated PD patients develop impulse control and repetitive behavior disorders (ICRBs) with punding being a well-defined stereotyped behavior (Evans et al., 2004; Lee et al., 2010). The behavioral abnormalities established in the *Fbxo7* cKO mice together with the observed increase in DAT, TH and DRD2 support the notion that loss of *Fbxo7* in glutamatergic neurons has a severe impact on dopamine homeostasis and results in an adaptive response of the dopaminergic pathway in the striatum that leads to aberrant psychomotor behavior. It is conceivable that there is a selective response in DRD2-expressing neurons over DRD1-expressing neurons in our animal model. Such a response has been shown in mice that were previously lesioned with 6-OHDA and treated with L-DOPA. Here, DRD2 MSNs had their spine density restored while D1R-MSNs did not (Suarez et al., 2014, 2016).

While there are no obvious signs of cell death in the *Fbxo7* cKO mice, we found microgliosis, increased levels of C1q and astrogliosis that may precede extensive cell loss as the neuropathology progresses. Gliosis has been observed in many neurodegenerative diseases and corresponding animal models (Verkhratsky et al., 2019). Microglia are pathology-sensing macrophages, that constantly scan the brain. Pathological changes or damage represent stimuli that trigger the transition of microglia from a resting to an activated state, in which they are able to remove cellular debris and secrete pro- and anti-inflammatory factors. In PD patients, PET tracers have been used to detect and monitor microglia and uncovered microglia activation in the early phase of the disease and found stable levels in later phases of the disease (Ho, 2019; Weiss et al., 2022). With Iba1 staining, we observed a significant increase in activated microglia in response to FBXO7 loss, underscoring the response of microglia to PD-inducing mechanisms.

Our quantitative synaptic analyses also uncovered complement 1q as an abnormally up-regulated factor upon loss of *Fbxo7*. C1q is the most upstream component of the complement cascade that ultimately leads to the formation of the membrane attack complex but also chemotactic and phagocytic signaling, and in synaptic pruning (Perry & O'Connor, 2008). Stevens and colleagues demonstrated this unexpected role for complement proteins in synapse elimination during development and, at the same time, found aberrant complement activation in the early phase of neurodegenerative disease models such as glaucoma and Alzheimer's disease (Hong et al., 2016; Stevens et al., 2007). Here, the authors demonstrated that microglia together with complement facilitated the removal of synapses and identified complement as a sensor for impending synaptic dysfunction or malfunction. Not only has C1q been associated with activation of pro-inflammatory microglia in the substantia nigra (SN), a newly published study compared the proteome of the SN from PD patients to healthy individuals and revealed the up-regulation of several complement proteins including C1q (Depboylu et al., 2011; Jang et al., 2022). While we observed up-regulated C1q, we did not observe any synaptic loss during the first 3 months in the lives of *Fbxo7* cKO mice as demonstrated by the synaptophysin/homer1 colocalization experiment. It is likely that the activation of complement and microglia will have an effect on synapses later in the disease as we found an increase in the localization of C1q at the synapses. Because of breeding restrictions however, we cannot analyze the mice at a more advanced stage.

Astrocytes are multifunctional cells and have been found to be crucial to brain homeostasis and neuronal functioning as they provide metabolic support. Astrocytes remove excess neurotransmitter and are involved in the proper formation of synapses and synaptic signaling. Astrocytes become reactive upon stimulation, which include pathological conditions of the brain such as trauma, neurodegeneration, or ischemia. They also play a role in PD by either directly contributing to the disease progression or by being activated in the course of the disease. Many studies observed an increase in astrogliosis in postmortem PD brain and in particular in areas of neurodegeneration and also in different mouse models (Niranjan, 2014; Rizor et al., 2019; Weiss et al., 2022). Interestingly, astrocytes receive input from activated microglia via cytokines (Liddelow et al., 2017).

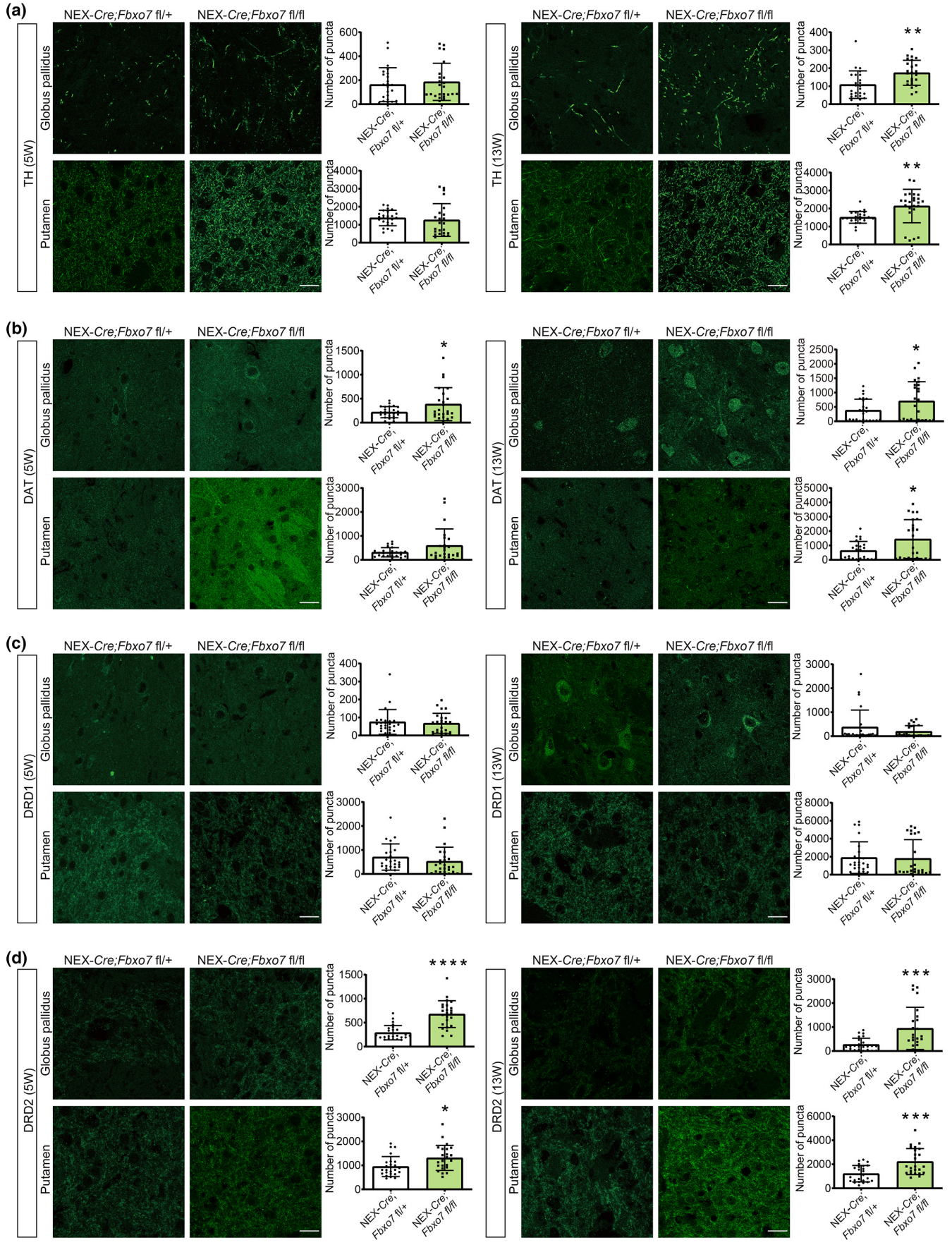

FIGURE 5 Examination of the dopaminergic pathway. (a–d) Representative images of coronal cryosections of 5- and 13-week-old NEX-*Cre*,*Fbxo7fl/+* (6 mice per age group) or NEX-*Cre*;*Fbxo7fl/fl* (6 mice per age group) forebrains that were subjected to immunostaining with the TH (a), DAT (b), DRD1 (c) or DRD2 (d) antibody, respectively. TH+, DAT+, DRD1+ or DRD2+ puncta in the putamen or globus pallidus per animal were included in the analysis using an ImageJ-based macro. 24 dots per graph represent the sum of 4 non-overlapping images of a section (of putamen or globus pallidus) per mouse. Student's *t*-test (*$p<0.5$, **$p<0.01$, ***$p<0.001$, ****$p<0.0001$, mean ± SEM). Magnification 63x, scale bar = 20 μm.

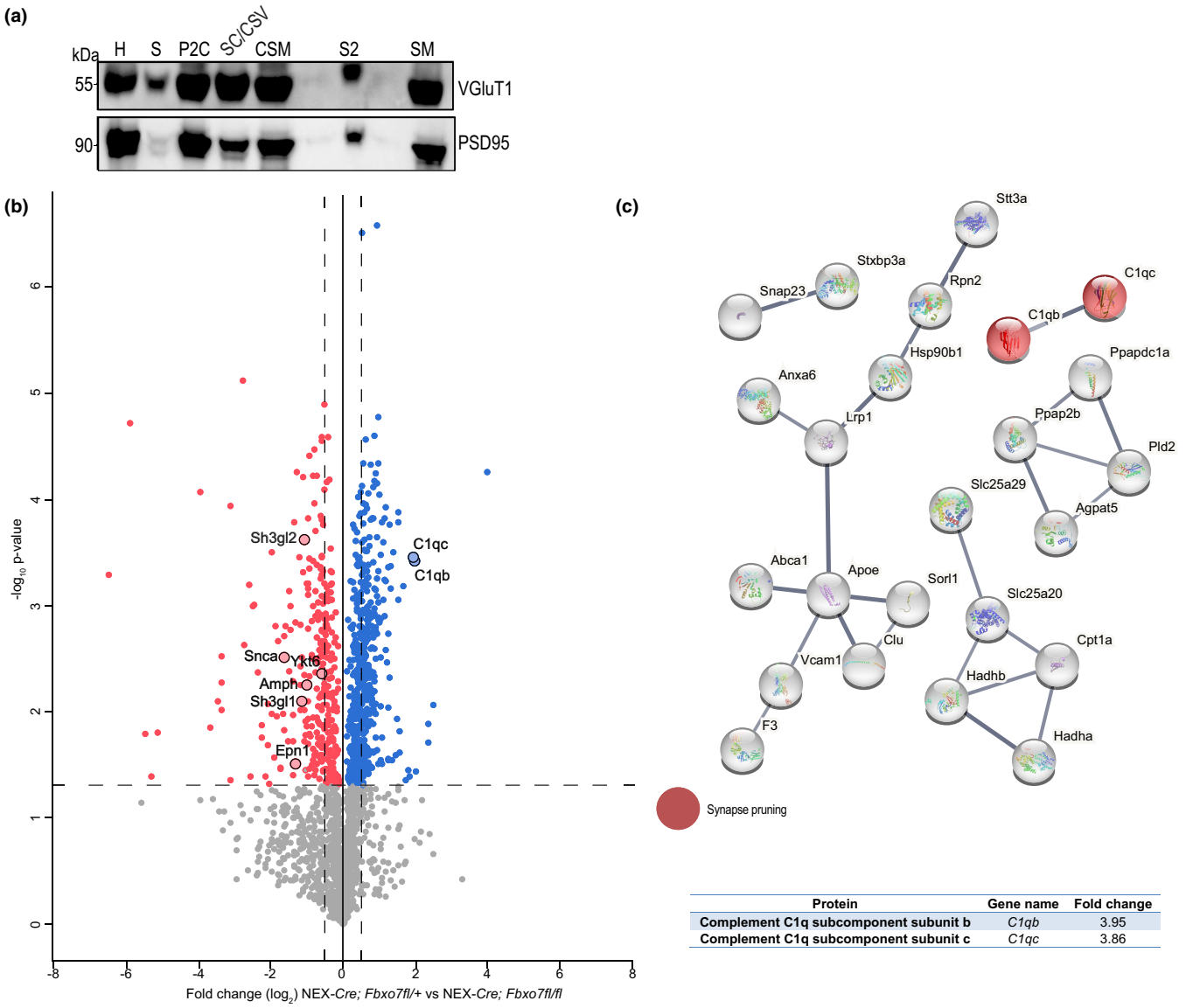

Protein	Gene name	Fold change
Complement C1q subcomponent subunit b	*C1qb*	3.95
Complement C1q subcomponent subunit c	*C1qc*	3.86

FIGURE 6 Quantitative mass spectrometry of striatal synaptic membranes in the *Fbxo7* cKO striatum (up-regulated proteins). (a) Striata from *Fbxo7* cKO or control mice were subjected to sucrose density gradient centrifugation to purify synaptic membranes followed by qMS. Fractions were analyzed with immunoblotting with the PSD95 and VGluT1 antibodies. H = homogenate, S = soluble fraction, SF = synaptosome fraction, SC/CSV = synaptic cytoplasm and coarse synaptic vesicles, CSM = coarse synaptic membrane, S2 = soluble fractions 2, SM = synaptic membranes. (b) Volcano plot displays quantified proteins of synaptic membrane fraction from *Fbxo7* cKO striata compared with control striata. X-axis displays $\log_2$ fold change of upregulated proteins (blue group) and downregulated proteins (red group) with vertical dashed lines representing threshold at −0.5 and 0.5. Y-axis displays log10 *p*-value with dashed line representing threshold at $p<0.05$. Proteins with statistically significant change lie above the dashed line. Singled out upregulated and downregulated proteins are the basis for analyses shown in Figures 7, 9 and 10. (c) STRING analysis of top 60 up-regulated proteins in *Fbxo7* cKO mice and fold change of complement 1qb and c.

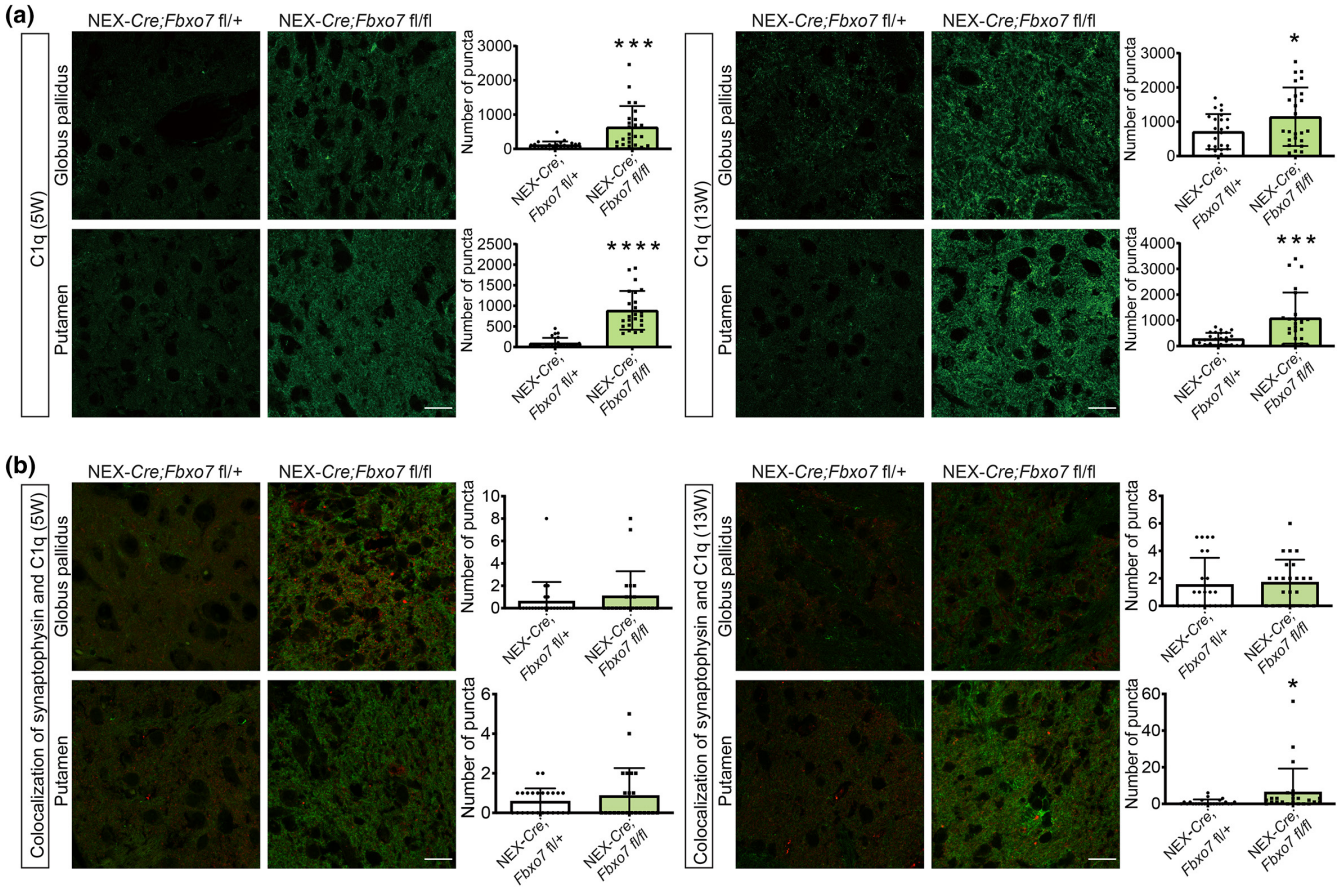

FIGURE 7 Significant up-regulation of C1q. (a) Representative images of coronal cryosections of 5- and 13-week-old NEX-*Cre*,*Fbxo7fl/+* (6 mice per age group) or NEX-*Cre*;*Fbxo7fl/fl* (6 mice per age group) forebrains that were subjected to immunostaining with the pan C1q antibody. C1q + puncta in the putamen or globus pallidus per animal were included in the analysis using an ImageJ-based macro. 24 dots per graph represent the sum of 4 non-overlapping images of a section (of putamen or globus pallidus) per mouse. Student's *t*-test (*$p < 0.5$, ***$p < 0.001$, ****$p < 0.0001$, mean ± SEM). Magnification 63×, scale bar = 20 μm. (b) Representative images of coronal cryosections of 5- and 13-week-old NEX-*Cre*,*Fbxo7fl/+* (6 mice per age group) or NEX-*Cre*;*Fbxo7fl/fl* (6 mice per age group) forebrains that were subjected to co-immunostaining with the pan C1q antibody together with the synaptophysin antibody. C1q + and synaptophysin+ puncta in the putamen or globus pallidus per animal were included in the co-localization analysis using an ImageJ-based macro. 24 dots per graph represent the sum of 24 non-overlapping images of a section (of putamen or globus pallidus) per mouse. Student's *t*-test (*$p < 0.5$, mean ± SEM). Magnification 63×, scale bar = 20 μm.

Pro-inflammatory cytokines in particular can result in reactive astrocytes (astrogliosis) that up-regulate GFAP and release e.g. tumor necrosis factor (TNF)-α (Niranjan, 2014; Rizor et al., 2019). In which way astrocytes contribute to the progression of the pathology in *Fbxo7* cKO mice remains elusive.

Aside from the reported changes in the dopaminergic pathway in the *Fbxo7* cKO mice, we also established changes in the glutamatergic and GABAergic pathway. We demonstrated the decrease in VGluT1 solely in the putamen, a change that is most certainly a direct effect of the genetic manipulations in the glutamatergic neurons. While we singled out the genetic manipulation of glutamatergic neurons in our study, alterations in glutamatergic transmission are common pathological features of PD, as the increase of VGluT1 has been also observed in postmortem putamen of PD patients as well as in the MPTP-treated monkey PD model (Kashani et al., 2007; Raju et al., 2008). The effect on VGluT1 levels in PD patients or the MPTP model is contrary to the findings in the *Fbxo7* cKO mice. But it is of note that our specific manipulation results in the increase in dopamine while brains of PD patients as well as MPTP models are characterized by low amounts of dopamine. Hence, the levels of VGluT1 and dopamine might be inversely correlated, which points to a homeostatic adaption in either system. Homeostatic plasticity has been demonstrated in a study by Fieblinger and colleagues who examined the corticostriatal connections in the 6-OHDA (hydroxydopamine) toxin model that is associated with dopamine depletion. Here, the direct and indirect pathway MSNs displayed differential changes in their excitability and indicated pathological changes of the glutamatergic synapse (Fieblinger et al., 2014).

The observed up-regulation of VGAT in the globus pallidus in the *Fbxo7* cKO mice might be secondary to the changes in the glutamatergic neurons and to the increased levels of dopamine and hence an adaptive response of the system. Plastic changes in the globus pallidus are also a consequence of PD treatment

(a)

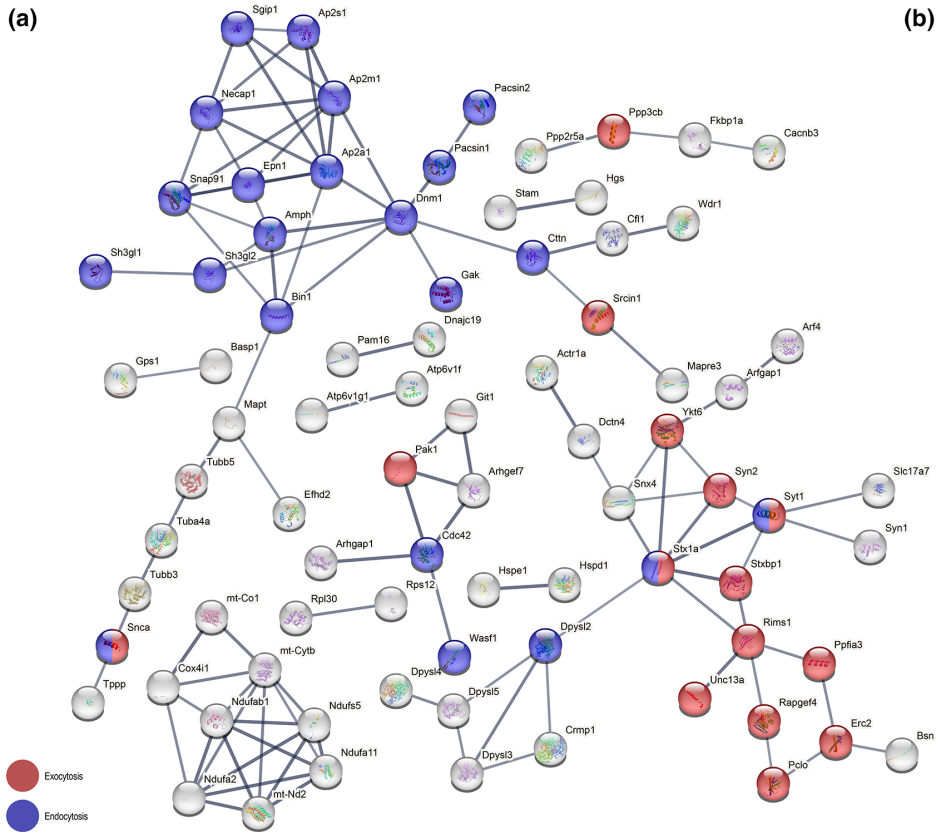

(b)

Protein	Gene name	Fold change
SH3-containing GRB2-like protein 3-interacting protein 1	*Sgip1*	0.41
AP-2 complex subunit sigma	*Ap2s1*	0.61
Adaptin ear-binding coat-associated protein 1	*Necap1*	0.72
AP-2 complex subunit mu	*Ap2m1*	0.71
Clathrin coat assembly protein AP180	*Snap91*	0.51
Epsin-1	*Epn1*	0.40
AP-2 complex subunit alpha-1	*Ap2a1*	0.73
Endophilin-A1	*Sh3gl1*	0.48
Endophilin-A2	*Sh3gl2*	0.45
Amphiphysin	*Amph*	0.50
Dynamin-1-like protein	*Dnm1*	0.80
Protein kinase C and casein kinase substrate in neurons protein 1	*Pacsin1*	0.52
Protein kinase C and casein kinase substrate in neurons protein 2	*Pacsin2*	0.26
Myc box-dependent-interacting protein 1	*Bin1*	0.55
Cyclin-G-associated kinase	*Gak*	0.69
Src substrate cortactin	*Cttn*	0.67
Cell division control protein 42 homolog	*Cdc42*	0.67
Wiskott-Aldrich syndrome protein family member 1	*Wasf1*	0.68
Dihydropyrimidinase-related protein 2	*Dpysl2*	0.74
Serine/threonine-protein phosphatase 2B catalytic subunit beta isoform	*Ppp3cb*	0.62
SRC kinase signaling inhibitor 1	*Srcin1*	0.66
Serine/threonine-protein kinase PAK 1	*Pak1*	0.65
α-synuclein	*Snca*	0.32
Synaptobrevin homolog YKT6	*Ykt6*	0.67
Synapsin-2	*Syn2*	0.56
Syntaxin-1A	*Stx1a*	0.67
Synaptotagmin-1	*Syt1*	0.71
Syntaxin-binding protein 1	*Stxbp1*	0.64
Regulating synaptic membrane exocytosis protein 1	*Rims1*	0.57
Protein unc-13 homolog A	*Unc13a*	0.73
Liprin-alpha-3	*Ppfia3*	0.66
Rap guanine nucleotide exchange factor 4	*Rapgef4*	0.71
Protein piccolo	*Pclo*	0.61
ERC protein 2	*Erc2*	0.64

FIGURE 8 Quantitative mass spectrometry of striatal synaptic membranes in the *Fbxo7* cKO striatum (down-regulated proteins). (a) STRING analysis of top 200 down-regulated proteins in *Fbxo7* cKO mice. (b) Fold change of exocytosis- and endocytosis-regulating proteins identified in top 200 down-regulated proteins.

with levodopa, which is on the one hand effective medication for Parkinson patients and on the other hand prone to cause side effects including levodopa-induced dyskinesia (LID). In a rat dyskinesia model, subjected to 6-OHDA lesioning followed by levodopa treatment, the researchers found hypertrophy of the globus pallidus areas after remittent administration of levodopa and in addition, an increase in GABA release in the globus pallidus upon acutely administered levodopa (Nishijima et al., 2020; Tomiyama et al., 2004). Interestingly, an optogenetics approach in mice, where GABAergic neurons of the globus pallidus were stimulated with a laser, resulted in hyperactivity and stereotypic behavior including circling and licking (Tian et al., 2018). Hence, it is reasonable to assume that a potential overactivation of GABAergic neurons in the globus pallidus in *Fbxo7* cKO mice contributes to the abnormal behavior.

Considering that the corticostriatal input into the striatum is critical to the function of the basal ganglia, it is not surprising that major processes of synaptic transmission are affected in the *Fbxo7* cKO striatum. We uncovered the down-regulation of the protein networks involved in exocytosis and endocytosis in these mice. Both deficits in exocytosis and endocytosis have been previously implicated in Parkinson disease (Zou et al., 2021) (Huang et al., 2019). Exocytosis at the presynaptic terminal facilitates the release of neurotransmitters from synaptic vesicles. Incoming action potentials induce calcium influx, which activates the SNARE complex. Components of the SNARE complex ultimately mediate the fusion of a specific pool of docked and primed synaptic vesicles, the so-called readily releasable pool (RRP), and the plasma membrane (Südhof, 2004). Among the changes in the exocytosis network, we validated the down-regulation of complexin1/2, α- and β-synuclein and YKT6.

Complexin1/2 are the two major isoforms expressed in the brain that bind to the SNARE complex and have been implicated in the priming of the RRP and calcium-dependent vesicle release (Yang et al., 2013). Although there is no direct genetic link of complexin1/2 with PD, different approaches in man and mouse revealed changes in complexin-1 levels and expression, respectively (Basso et al., 2004; Gispert et al., 2015). Also, loss of complexin-1 in mice has a clear effect on motor coordination and locomotion (Glynn et al., 2005).

α- and β-synuclein are present in presynaptic terminals and owing to their homology are likely to have redundant functions. *SNCA/SNCB* dKO mice revealed no essential role for these proteins in exocytosis machinery but did affect the level of striatal dopamine, so the authors came to the conclusion that α- and β-synuclein rather play a role in the long-term maintenance of the synapse and, in addition α-synuclein appears to act as a chaperone in SNARE complex assembly (Jacqueline Burré et al., 2014; Chandra et al., 2004). Aside

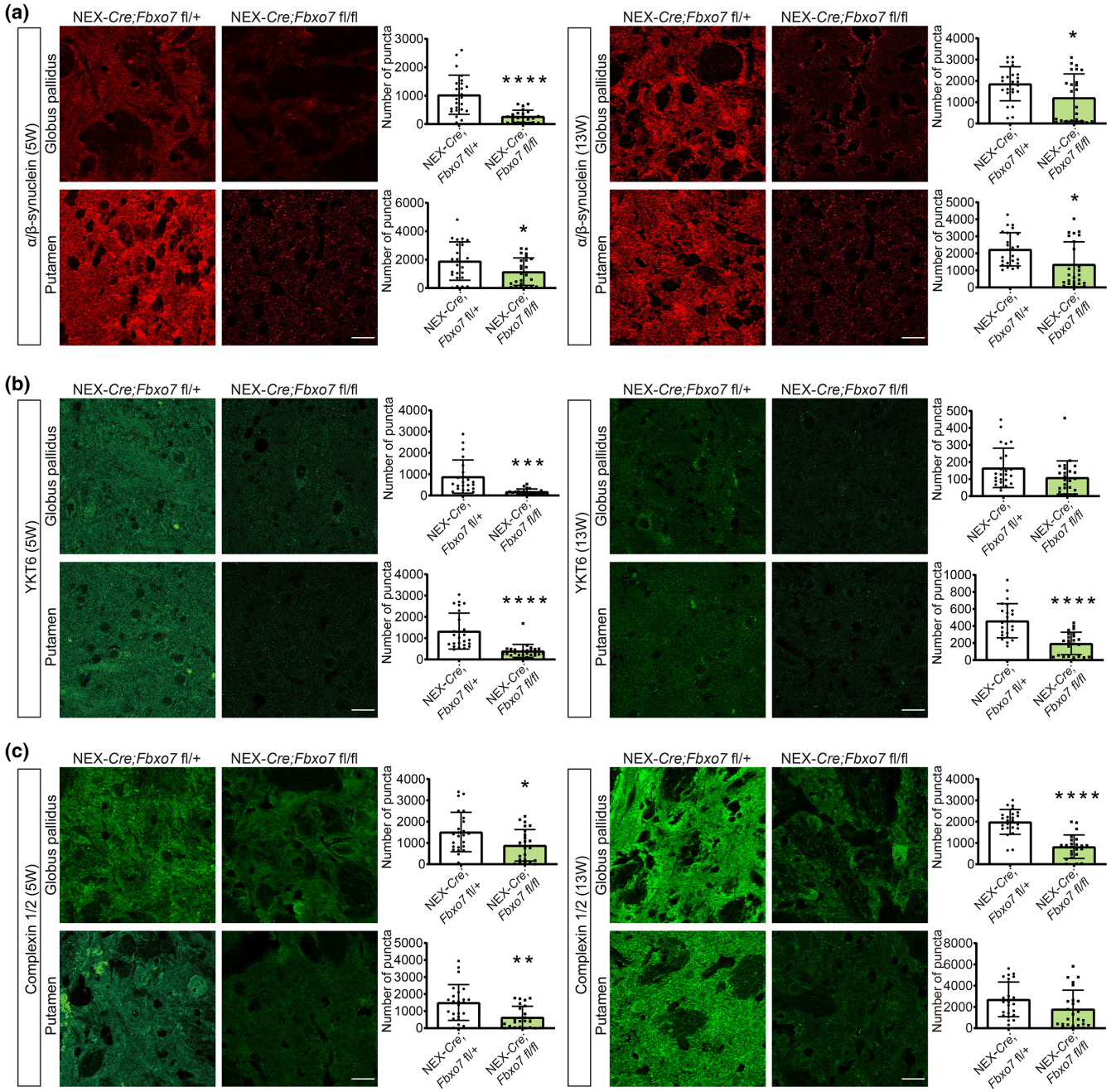

FIGURE 9 Down-regulation of exocytosis network in NEX-*Cre*;*Fbxo7fl/fl mice*. Representative images of coronal cryosections of 5- and 13-week-old NEX-*Cre*, *Fbxo7fl/+* (6 mice per age group) or NEX-*Cre*;*Fbxo7fl/fl* (6 mice per age group) forebrains that were subjected to immunostaining with the α/β-synuclein (a), YKT6 (b) or complexin1/2 (c) antibody, respectively. α/β-synuclein+, YKT6+ or complexin1/2+ puncta in the putamen or globus pallidus per animal were included in the analysis using an ImageJ-based macro. 24 dots per graph represent the sum of 4 non-overlapping images of a section (of putamen or globus pallidus) per mouse. Student's test (*$p<0.5$, **$p<0.01$ ***$p<0.001$, ****$p<0.0001$, mean ± SEM). Magnification 63×, scale bar = 20 μm.

from disease-causing mutations, *SNCA* has also been identified as a risk gene for PD in GWAS (Chang et al., 2017; Nalls et al., 2014).

YKT6 acts as a v-SNARE in the vesicle transport from ER to Golgi and has an interesting functional relationship with α-synuclein. Two studies have shown that YKT6 relieves α-synuclein-triggered blockage of ER-Golgi trafficking (Cooper et al., 2006; Thayanidhi et al., 2010). During proteostasis, when aggregated or accumulated proteins require clearance, YKT6 was found to enhance the clearance process, while α-synuclein was found to counteract this process by binding to YKT6 in PD neurons (Cuddy et al., 2019).

The validated down-regulated proteins involved in endocytosis were amphiphysin, endophilin A1 and epsin-1. Endocytosis at the presynaptic terminal serves the retrieval of synaptic vesicles. While there are different routes of vesicles retrieval (Chanaday et al., 2019), the proteins that we have identified in the qMS analysis participate in clathrin-mediated endocytosis, a process that is

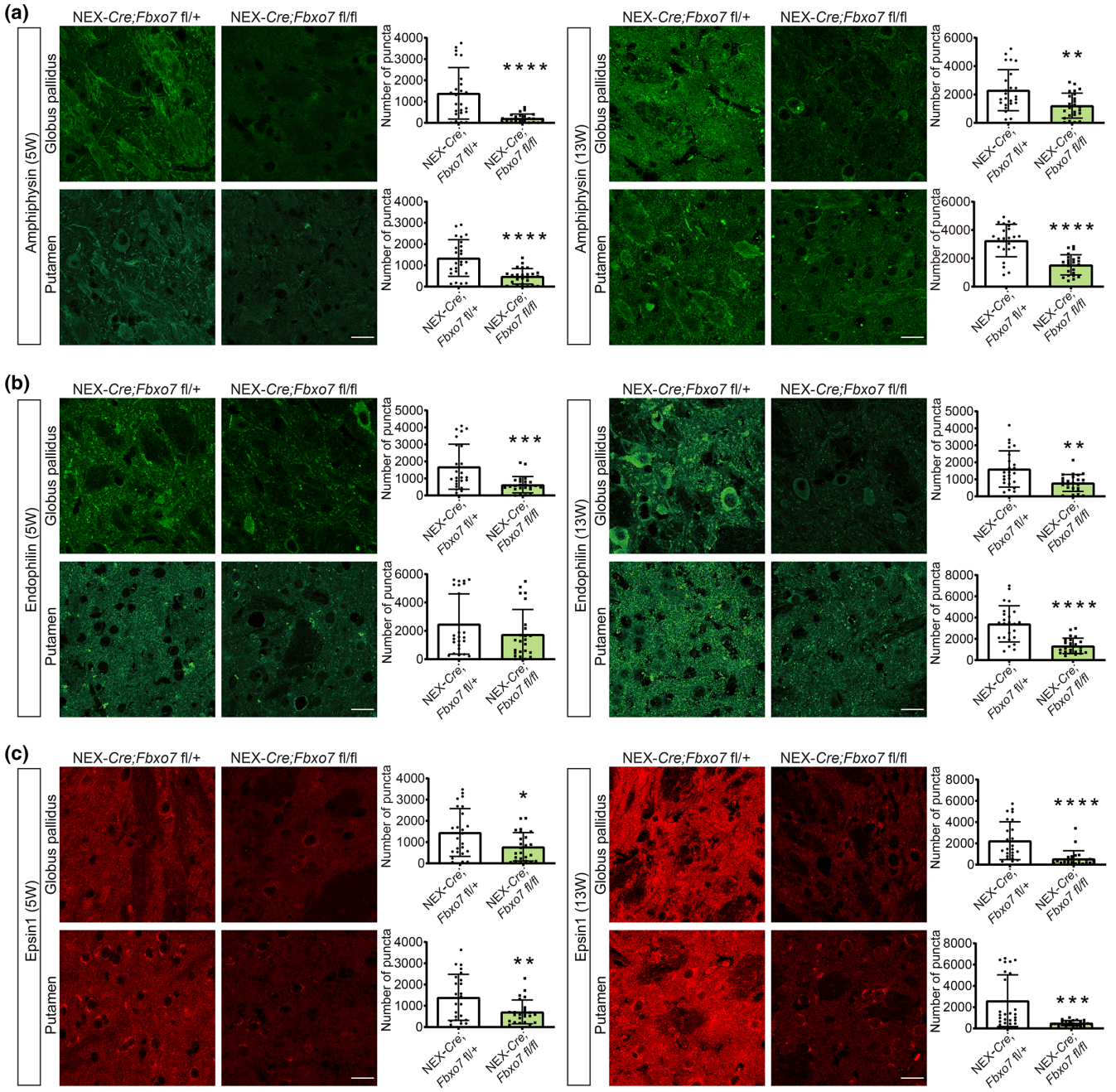

FIGURE 10 Down-regulation of endocytosis network in NEX-*Cre*;*Fbxo7fl/fl mice*. Representative images of coronal cryosections of 5- and 13-week-old NEX-*Cre*, *Fbxo7fl/+* (6 mice per age group) or NEX-*Cre*;*Fbxo7fl/fl* (6 mice per age group) forebrains that were subjected to immunostaining with the amphiphysin (a), endophilin (b) or epsin-1 (c) antibody, respectively. Amphiphysin+, endophilin+ or epsin-1 + puncta in the putamen or globus pallidus per animal were included in the analysis using an ImageJ-based macro. 24 dots per graph represent the sum of 4 non-overlapping images of a section (of putamen or globus pallidus) per mouse. Student's *t*-test (*$p < 0.5$,**$p < 0.01$ ***$p < 0.001$, ****$p < 0.0001$, mean ± SEM). Magnification 63×, scale bar = 20 μm.

initiated by the coating of the membrane with clathrin. Epsin-1 is an alternative adaptor for clathrin-mediated membrane invagination (Chen et al., 1998; Itoh & De Camilli, 2006). The activity of amphiphysin and endophilin A1 drives the progression of endocytosis (Zou et al., 2021) as both proteins harbor BAR domains, which induce membrane curvature and mediate binding to curved membranes. In addition, amphiphysin is a binding partner of endophilin (Micheva et al., 1997). Endophilin A1 has been implicated in Parkinson disease due to the identification of *SH3GL2* as PD risk loci (Chang et al., 2017). Interestingly, endophilin-1 is also a substrate of LRRK2, a kinase whose mutations are causative for a genetic variant of Parkinson disease (Arranz et al., 2015).

As a consequence of deletion of *Fbxo7* in glutamatergic forebrain neurons in mice, behavioral changes go hand in hand with changes in different neurotransmitter systems and with molecular changes at the striatal synapse. FBXO7 acts as the substrate-recruiting subunit of an

SCF (Skp1/cullin-1/F-box protein)-type E3 ubiquitin ligase and the lack of ubiquitination of specific substrates might have adversarial effects on pathways the substrates are intertwined with. While we can exclude an association with α- or β-synuclein, YKT6, endophilin A1, epsin-1 and amphiphysin (unpublished data), it is conceivable that other proteins of the networks are substrates of FBXO7. Future research is required to address the question of how loss of the biochemical activity of the E3 ubiquitin ligase FBXO7-SCF leads to these massive changes.

In conclusion, the results of the present study suggest that FBXO7 is crucial for corticostriatal projections, the synaptic integrity of the striatum and the nigrostriatal dopamine system in the mouse. The neuropathological changes observed in the striatum in *Fbxo7* cKO mice are associated with general hyperactivity and behavioral stereotypies resembling the psychomotor and psychiatric signs seen in PARK15 patients or PD patients receiving levodopa treatment.

AUTHOR CONTRIBUTIONS

J.B.W., S.J. and S.V. performed experiments and analyzed data; E.D., A.R. and H.E. carried out and supervised LABORAS; L.T. and P.L. performed and supervised HPLC analysis, respectively; C.P. carried out quantitative mass spectrometry analysis; J.B.W., J.B.S and J.S. obtained funding, J.B.W. co-wrote the manuscript; J.S. designed study, supervised experiments and wrote manuscript.

ACKNOWLEDGEMENTS

This work was funded by the Deutsche Forschungsgemeinschaft (DFG, German Research Foundation – 368482240/GRK2416 and STE1117/10-1, STE1117/14-1), START program, RWTH Aachen (JS), and the GGNB Excellence Stipend, University of Göttingen (SV). We thank Sandra Goebbels and Klaus-Armin Nave (MPI for Multidisciplinary Sciences, Göttingen) for providing the NEX-*Cre* driver mouse line. Open Access funding enabled and organized by Projekt DEAL.

CONFLICT OF INTEREST STATEMENT

Judith Stegmüller is a former Editor of Journal of Neurochemistry. Jörg B. Schulz is a former Editor-in-Chief of Journal of Neurochemistry. The authors declare no competing financial interest.

PEER REVIEW

The peer review history for this article is available at https://www.webofscience.com/api/gateway/wos/peer-review/10.1111/jnc.15962.

DATA AVAILABILITY STATEMENT

Data have been deposited to the ProteomeXchange consortium under identifier PXD044119: https://www.ebi.ac.uk/pride/archive/projects/PXD044119 (Project DOI: 10.1111/jnc15962).

ORCID

Lars Tatenhorst https://orcid.org/0000-0002-6690-688X
Paul Lingor https://orcid.org/0000-0001-9362-7096
Jörg B. Schulz https://orcid.org/0000-0002-8903-0593
Judith Stegmüller https://orcid.org/0000-0003-4172-7778

REFERENCES

Arranz, A. M., Delbroek, L., Van Kolen, K., Guimarães, M. R., Mandemakers, W., Daneels, G., Matta, S., Calafate, S., Shaban, H., Baatsen, P., De Bock, P. J., Gevaert, K., Vanden Berghe, P., Verstreken, P., De Strooper, B., & Moechars, D. (2015). LRRK2 functions in synaptic vesicle endocytosis through a kinase-dependent mechanism. *Journal of Cell Science*, *128*(3), 541–552. https://doi.org/10.1242/jcs.158196

Basso, M., Giraudo, S., Corpillo, D., Bergamasco, B., Lopiano, L., & Fasano, M. (2004). Proteome analysis of human substantia nigra in Parkinson's disease. *Proteomics*, *4*(12), 3943–3952. https://doi.org/10.1002/pmic.200400848

Bidesi, N. S. R., Vang Andersen, I., Windhorst, A. D., Shalgunov, V., & Herth, M. M. (2021). The role of neuroimaging in Parkinson's disease. *Journal of Neurochemistry*, *159*(4), 660–689. https://doi.org/10.1111/jnc.15516

Burré, J., Sharma, M., & Südhof, T. C. (2014). α-Synuclein assembles into higher-order multimers upon membrane binding to promote SNARE complex formation. *Proceedings of the National Academy of Sciences*, *111*(40), E4274–E4283. https://doi.org/10.1073/pnas.1416598111

Burré, J., Sharma, M., Tsetsenis, T., Buchman, V., Etherton, M. R., & Südhof, T. C. (2010). Alpha-synuclein promotes SNARE-complex assembly in vivo and in vitro. *Science*, *329*(5999), 1663–1667. https://doi.org/10.1126/science.1195227

Calabresi, P., Picconi, B., Tozzi, A., & Di Filippo, M. (2007). Dopamine-mediated regulation of corticostriatal synaptic plasticity. *Trends in Neurosciences*, *30*(5), 211–219. https://doi.org/10.1016/j.tins.2007.03.001

Calo, L., Wegrzynowicz, M., Santivañez-Perez, J., & Grazia Spillantini, M. (2016). Synaptic failure and α-synuclein. *Movement Disorders*, *31*(2), 169–177.

Chanaday, N. L., Cousin, M. A., Milosevic, I., Watanabe, S., & Morgan, J. R. (2019). The synaptic vesicle cycle revisited: New insights into the modes and mechanisms. *The Journal of Neuroscience*, *39*(42), 8209–8216. https://doi.org/10.1523/jneurosci.1158-19.2019

Chandra, S., Fornai, F., Kwon, H. B., Yazdani, U., Atasoy, D., Liu, X., Hammer, R. E., Battaglia, G., German, D. C., Castillo, P. E., & Südhof, T. C. (2004). Double-knockout mice for α- and β-synucleins: Effect on synaptic functions. *Proceedings of the National Academy of Sciences*, *101*(41), 14966–14971. https://doi.org/10.1073/pnas.0406283101

Chang, D., Nalls, M. A., Hallgrímsdóttir, I. B., Hunkapiller, J., van der Brug, M., Cai, F., International Parkinson's Disease Genomics Consortium; 23 and Me Research Team, Kerchner, G. A., Ayalon, G., Bingol, B., Sheng, M., Hinds, D., Behrens, T. W., Singleton, A. B., Bhangale, T. R., & Graham, R. R. (2017). A meta-analysis of genome-wide association studies identifies 17 new Parkinson's disease risk loci. *Nature Genetics*, *49*(10), 1511–1516. https://doi.org/10.1038/ng.3955

Chen, H., Fre, S., Slepnev, V. I., Capua, M. R., Takei, K., Butler, M. H., Di Fiore, P. P., & De Camilli, P. (1998). Epsin is an EH-domain-binding protein implicated in clathrin-mediated endocytosis. *Nature*, *394*(6695), 793–797. https://doi.org/10.1038/29555

Cinque, S., Zoratto, F., Poleggi, A., Leo, D., Cerniglia, L., Cimino, S., Tambelli, R., Alleva, E., Gainetdinov, R. R., Laviola, G., & Adriani, W. (2018). Behavioral phenotyping of dopamine transporter knockout rats: Compulsive traits, motor stereotypies, and anhedonia. *Frontiers in Psychiatry*, *9*, 43. https://doi.org/10.3389/fpsyt.2018.00043

Cooper, A. A., Gitler, A. D., Cashikar, A., Haynes, C. M., Hill, K. J., Bhullar, B., Liu, K., Xu, K., Strathearn, K. E., Liu, F., Cao, S., Caldwell, K. A., Caldwell, G. A., Marsischky, G., Kolodner, R. D., Labaer, J., Rochet, J. C., Bonini, N. M., & Lindquist, S. (2006). Alpha-synuclein blocks ER-Golgi traffic and Rab1 rescues neuron loss in Parkinson's models. *Science*, *313*(5785), 324–328. https://doi.org/10.1126/science.1129462

Correa-Vela, M., Lupo, V., Montpeyó, M., Sancho, P., Marcé-Grau, A., Hernández-Vara, J., Darling, A., Jenkins, A., Fernández-Rodríguez,

S., Tello, C., Ramírez-Jiménez, L., Pérez, B., Sánchez-Montáñez, Á., Macaya, A., Sobrido, M. J., Martinez-Vicente, M., Pérez-Dueñas, B., & Espinós, C. (2020). Impaired proteasome activity and neurodegeneration with brain iron accumulation in FBXO7 defect. *Annals of Clinical Translational Neurology*, *7*, 1436–1442. https://doi.org/10.1002/acn3.51095

Cuddy, L. K., Wani, W. Y., Morella, M. L., Pitcairn, C., Tsutsumi, K., Fredriksen, K., Justman, C. J., Grammatopoulos, T. N., Belur, N. R., Zunke, F., Subramanian, A., Affaneh, A., Lansbury, P. T., Jr., & Mazzulli, J. R. (2019). Stress-induced cellular clearance is mediated by the SNARE protein ykt6 and disrupted by alpha-synuclein. *Neuron*, *104*(5), 869–884 e811. https://doi.org/10.1016/j.neuron.2019.09.001

Depboylu, C., Schäfer, M. K.-H., Arias-Carrión, O., Oertel, W. H., Weihe, E., & Höglinger, G. U. (2011). Possible involvement of complement factor C1q in the clearance of extracellular neuromelanin from the substantia nigra in Parkinson disease. *Journal of Neuropathology & Experimental Neurology*, *70*(2), 125–132. https://doi.org/10.1097/NEN.0b013e31820805b9

Dere, E., Dahm, L., Lu, D., Hammerschmidt, K., Ju, A., Tantra, M., Kästner, A., Chowdhury, K., & Ehrenreich, H. (2014). Heterozygous ambra1 deficiency in mice: A genetic trait with autism-like behavior restricted to the female gender. *Frontiers in Behavioral Neuroscience*, *8*, 181. https://doi.org/10.3389/fnbeh.2014.00181

Deutsch, E. W., Bandeira, N., Perez-Riverol, Y., Sharma, V., Carver, J. J., Mendoza, L., Kundu, D. J., Wang, S., Bandla, C., Kamatchinathan, S., Hewapathirana, S., Pullman, B. S., Wertz, J., Sun, Z., Kawano, S., Okuda, S., Watanabe, Y., MacLean, B., MacCoss, M. J., … Vizcaíno, J. A. (2023). The ProteomeXchange consortium at 10 years: 2023 update. *Nucleic Acids Research*, *51*(D1), D1539–D1548. https://doi.org/10.1093/nar/gkac1040

Di Fonzo, A., Dekker, M. C., Montagna, P., Baruzzi, A., Yonova, E. H., Correia Guedes, L., Szczerbinska, A., Zhao, T., Dubbel-Hulsman, L. O., Wouters, C. H., de Graaff, E., Oyen, W. J., Simons, E. J., Breedveld, G. J., Oostra, B. A., Horstink, M. W., & Bonifati, V. (2009). FBXO7 mutations cause autosomal recessive, early-onset parkinsonian-pyramidal syndrome. *Neurology*, *72*(3), 240–245. https://doi.org/10.1212/01.wnl.0000338144.10967.2b

El-Kordi, A., Winkler, D., Hammerschmidt, K., Kästner, A., Krueger, D., Ronnenberg, A., Ritter, C., Jatho, J., Radyushkin, K., Bourgeron, T., Fischer, J., Brose, N., & Ehrenreich, H. (2013). Development of an autism severity score for mice using Nlgn4 null mutants as a construct-valid model of heritable monogenic autism. *Behavioural Brain Research*, *251*, 41–49. https://doi.org/10.1016/j.bbr.2012.11.016

Eshuis, S. A., Jager, P. L., Maguire, R. P., Jonkman, S., Dierckx, R. A., & Leenders, K. L. (2009). Direct comparison of FP-CIT SPECT and F-DOPA PET in patients with Parkinson's disease and healthy controls. *European Journal of Nuclear Medicine and Molecular Imaging*, *36*(3), 454–462. https://doi.org/10.1007/s00259-008-0989-5

Evans, A. H., Katzenschlager, R., Paviour, D., O'Sullivan, J. D., Appel, S., Lawrence, A. D., & Lees, A. J. (2004). Punding in Parkinson's disease: Its relation to the dopamine dysregulation syndrome. *Movement Disorders*, *19*(4), 397–405. https://doi.org/10.1002/mds.20045

Fieblinger, T., Graves, S. M., Sebel, L. E., Alcacer, C., Plotkin, J. L., Gertler, T. S., Chan, C. S., Heiman, M., Greengard, P., Cenci, M. A., & Surmeier, D. J. (2014). Cell type-specific plasticity of striatal projection neurons in parkinsonism and L-DOPA-induced dyskinesia. *Nature Communications*, *5*, 5316. https://doi.org/10.1038/ncomms6316

Gainetdinov, R. R., Jones, S. R., Fumagalli, F., Wightman, R. M., & Caron, M. G. (1998). Re-evaluation of the role of the dopamine transporter in dopamine system homeostasis. *Brain Research. Brain Research Reviews*, *26*(2–3), 148–153. Retrieved from http://www.ncbi.nlm.nih.gov/pubmed/9651511

Gerfen, C. R., & Surmeier, D. J. (2011). Modulation of striatal projection systems by dopamine. *Annual Review of Neuroscience*, *34*, 441–466. https://doi.org/10.1146/annurev-neuro-061010-113641

Giros, B., Jaber, M., Jones, S. R., Wightman, R. M., & Caron, M. G. (1996). Hyperlocomotion and indifference to cocaine and amphetamine in mice lacking the dopamine transporter. *Nature*, *379*(6566), 606–612. https://doi.org/10.1038/379606a0

Gispert, S., Kurz, A., Brehm, N., Rau, K., Walter, M., Riess, O., & Auburger, G. (2015). Complexin-1 and Foxp1 expression changes are novel brain effects of alpha-synuclein pathology. *Molecular Neurobiology*, *52*(1), 57–63. https://doi.org/10.1007/s12035-014-8844-0

Glick, S. D., Jerussi, T. P., Water, D. H., & Green, J. P. (1974). Amphetamine-induced changes in striatal dopamine and acetylcholine levels and relationship to rotation (circling behavior) in rats. *Biochemical Pharmacology*, *23*(22), 3223–3225. Retrieved from http://www.ncbi.nlm.nih.gov/pubmed/4474884

Glynn, D., Drew, C. J., Reim, K., Brose, N., & Morton, A. J. (2005). Profound ataxia in complexin I knockout mice masks a complex phenotype that includes exploratory and habituation deficits. *Human Molecular Genetics*, *14*(16), 2369–2385. https://doi.org/10.1093/hmg/ddi239

Goebbels, S., Bormuth, I., Bode, U., Hermanson, O., Schwab, M. H., & Nave, K. A. (2006). Genetic targeting of principal neurons in neocortex and hippocampus of NEX-Cre mice. *Genesis*, *44*(12), 611–621. https://doi.org/10.1002/dvg.20256

Hawryluk, M. J., Keyel, P. A., Mishra, S. K., Watkins, S. C., Heuser, J. E., & Traub, L. M. (2006). Epsin 1 is a polyubiquitin-selective clathrin-associated sorting protein. *Traffic*, *7*(3), 262–281. https://doi.org/10.1111/j.1600-0854.2006.00383.x

Hilker, R., Schweitzer, K., Coburger, S., Ghaemi, M., Weisenbach, S., Jacobs, A. H., Rudolf, J., Herholz, K., & Heiss, W. D. (2005). Nonlinear progression of Parkinson disease as determined by serial positron emission tomographic imaging of striatal fluorodopa F 18 activity. *Archives of Neurology*, *62*(3), 378–382. https://doi.org/10.1001/archneur.62.3.378

Ho, M. S. (2019). Microglia in Parkinson's disease. In A. Verkhratsky, M. S. Ho, R. Zorec, & V. Parpura (Eds.), *Neuroglia in neurodegenerative diseases* (pp. 335–353). Springer Singapore.

Hong, S., Beja-Glasser, V. F., Nfonoyim, B. M., Frouin, A., Li, S., Ramakrishnan, S., Merry, K. M., Shi, Q., Rosenthal, A., Barres, B. A., Lemere, C. A., Selkoe, D. J., & Stevens, B. (2016). Complement and microglia mediate early synapse loss in Alzheimer mouse models. *Science*, *352*(6286), 712–716. https://doi.org/10.1126/science.aad8373

Huang, M., Wang, B., Li, X., Fu, C., Wang, C., & Kang, X. (2019). α-Synuclein: A multifunctional player in exocytosis, endocytosis, and vesicle recycling. *Frontiers in Neuroscience*, *13*, 28. https://doi.org/10.3389/fnins.2019.00028

Imbriani, P., Martella, G., Bonsi, P., & Pisani, A. (2022). Oxidative stress and synaptic dysfunction in rodent models of Parkinson's disease. *Neurobiology of Disease*, *173*, 105851. https://doi.org/10.1016/j.nbd.2022.105851

Ippolito, D. M., & Eroglu, C. (2010). Quantifying synapses: An immunocytochemistry-based assay to quantify synapse number. *Journal of Visualized Experiments*, (45). https://doi.org/10.3791/2270

Itoh, T., & De Camilli, P. (2006). BAR, F-BAR (EFC) and ENTH/ANTH domains in the regulation of membrane–cytosol interfaces and membrane curvature. *Biochimica et Biophysica Acta (BBA)—Molecular and Cell Biology of Lipids*, *1761*(8), 897–912. https://doi.org/10.1016/j.bbalip.2006.06.015

Jang, Y., Pletnikova, O., Troncoso, J. C., Pantelyat, A. Y., Dawson, T. M., Rosenthal, L. S., & Na, C. H. (2022). Mass spectrometry-based proteomics analysis of human substantia nigra from Parkinson's disease patients identifies multiple pathways potentially involved in the disease. *Molecular & Cellular Proteomics*, *100452*. https://doi.org/10.1016/j.mcpro.2022.100452

Jin, X., An, L., Hao, S., Liu, Q., Zhang, Q., Wang, X., Feng, X., Zhang, C., Cao, X., Yan, Y., & Ma, X. (2020). Compound heterozygous variants of the FBXO7 gene resulting in infantile-onset Parkinsonian-pyramidal syndrome in siblings of a Chinese family. *Journal of Clinical Laboratory Analysis*, *34*(8), e23324. https://doi.org/10.1002/jcla.23324

Kashani, A., Betancur, C., Giros, B., Hirsch, E., & El Mestikawy, S. (2007). Altered expression of vesicular glutamate transporters VGLUT1 and VGLUT2 in Parkinson disease. *Neurobiology of Aging*, *28*(4), 568–578. https://doi.org/10.1016/j.neurobiolaging.2006.02.010

Kramer, P. F., Christensen, C. H., Hazelwood, L. A., Dobi, A., Bock, R., Sibley, D. R., Mateo, Y., & Alvarez, V. A. (2011). Dopamine D2 receptor overexpression alters behavior and physiology in Drd2-EGFP mice. *The Journal of Neuroscience*, *31*(1), 126–132. https://doi.org/10.1523/JNEUROSCI.4287-10.2011

Lee, J. Y., Kim, J. M., Kim, J. W., Cho, J., Lee, W. Y., Kim, H. J., & Jeon, B. S. (2010). Association between the dose of dopaminergic medication and the behavioral disturbances in Parkinson disease. *Parkinsonism & Related Disorders*, *16*(3), 202–207. https://doi.org/10.1016/j.parkreldis.2009.12.002

Leo, D., Sukhanov, I., Zoratto, F., Illiano, P., Caffino, L., Sanna, F., Messa, G., Emanuele, M., Esposito, A., Dorofeikova, M., Budygin, E. A., Mus, L., Efimova, E. V., Niello, M., Espinoza, S., Sotnikova, T. D., Hoener, M. C., Laviola, G., Fumagalli, F., … Gainetdinov, R. R. (2018). Pronounced hyperactivity, cognitive dysfunctions, and BDNF dysregulation in dopamine transporter knock-out rats. *The Journal of Neuroscience*, *38*(8), 1959–1972. https://doi.org/10.1523/JNEUROSCI.1931-17.2018

Liddelow, S. A., Guttenplan, K. A., Clarke, L. E., Bennett, F. C., Bohlen, C. J., Schirmer, L., Bennett, M. L., Münch, A. E., Chung, W. S., Peterson, T. C., Wilton, D. K., Frouin, A., Napier, B. A., Panicker, N., Kumar, M., Buckwalter, M. S., Rowitch, D. H., Dawson, V. L., Dawson, T. M., … Barres, B. A. (2017). Neurotoxic reactive astrocytes are induced by activated microglia. *Nature*, *541*(7638), 481–487. https://doi.org/10.1038/nature21029

Lohmann, E., Coquel, A. S., Honoré, A., Gurvit, H., Hanagasi, H., Emre, M., Leutenegger, A. L., Drouet, V., Sahbatou, M., Guven, G., Erginel-Unaltuna, N., Deleuze, J. F., Lesage, S., & Brice, A. (2015). A new F-box protein 7 gene mutation causing typical Parkinson's disease. *Movement Disorders*, *30*(8), 1130–1133. https://doi.org/10.1002/mds.26266

Lorenzo-Betancor, O., Lin, Y. H., Samii, A., Jayadev, S., Kim, H. M., Longfellow, K., Distad, B. J., Yearout, D., Mata, I. F., & Zabetian, C. P. (2020). Novel compound heterozygous FBXO7 mutations in a family with early onset Parkinson's disease. *Parkinsonism & Related Disorders*, *80*, 142–147. https://doi.org/10.1016/j.parkreldis.2020.09.035

Lovinger, D. M. (2010). Neurotransmitter roles in synaptic modulation, plasticity and learning in the dorsal striatum. *Neuropharmacology*, *58*(7), 951–961. https://doi.org/10.1016/j.neuropharm.2010.01.008

McNew, J. A., Sogaard, M., Lampen, N. M., Machida, S., Ye, R. R., Lacomis, L., Tempst, P., Rothman, J. E., & Söllner, T. H. (1997). Ykt6p, a prenylated SNARE essential for endoplasmic reticulum-Golgi transport. *The Journal of Biological Chemistry*, *272*(28), 17776–17783. https://doi.org/10.1074/jbc.272.28.17776

Micheva, K. D., Ramjaun, A. R., Kay, B. K., & McPherson, P. S. (1997). SH3 domain-dependent interactions of endophilin with amphiphysin. *FEBS Letters*, *414*(2), 308–312. https://doi.org/10.1016/S0014-5793(97)01016-8

Nalls MA, Pankratz N, Lill CM, Do CB, Hernandez DG, Saad M, DeStefano AL, Kara E, Bras J, Sharma M, Schulte C, Keller MF, Arepalli S, Letson C, Edsall C, Stefansson H, Liu X, Pliner H, Lee JH, …, Singleton AB. Large-scale meta-analysis of genome-wide association data identifies six new risk loci for Parkinson's disease. *Nature Genetics*. 2014;*46*(9):989-93. https://doi.org/10.1038/ng.3043

Niranjan, R. (2014). The role of inflammatory and oxidative stress mechanisms in the pathogenesis of Parkinson's disease: Focus on astrocytes. *Molecular Neurobiology*, *49*(1), 28–38. https://doi.org/10.1007/s12035-013-8483-x

Nishijima, H., Mori, F., Arai, A., Zhu, G., Wakabayashi, K., Okada, M., Ueno, S., Ichinohe, N., Suzuki, C., Kon, T., & Tomiyama, M. (2020). GABA storage and release in the medial globus pallidus in L-DOPA-induced dyskinesia priming. *Neurobiology of Disease*, *143*, 104979. https://doi.org/10.1016/j.nbd.2020.104979

Perez-Riverol, Y., Bai, J., Bandla, C., García-Seisdedos, D., Hewapathirana, S., Kamatchinathan, S., Kundu, D. J., Prakash, A., Frericks-Zipper, A., Eisenacher, M., Walzer, M., Wang, S., Brazma, A., & Vizcaíno, J. A. (2022). The PRIDE database resources in 2022: a hub for mass spectrometry-based proteomics evidences. *Nucleic Acids Research*, *50*(D1), D543–D552. https://doi.org/10.1093/nar/gkab1038

Perry, V. H., & O'Connor, V. (2008). C1q: The perfect complement for a synaptic feast? *Nature Reviews Neuroscience*, *9*(11), 807–811. https://doi.org/10.1038/nrn2394

Polymeropoulos, M. H., Lavedan, C., Leroy, E., Ide, S. E., Dehejia, A., Dutra, A., Pike, B., Root, H., Rubenstein, J., Boyer, R., Stenroos, E. S., Chandrasekharappa, S., Athanassiadou, A., Papapetropoulos, T., Johnson, W. G., Lazzarini, A. M., Duvoisin, R. C., Di Iorio, G., Golbe, L. I., & Nussbaum, R. L. (1997). Mutation in the alpha-synuclein gene identified in families with Parkinson's disease. *Science*, *276*(5321), 2045–2047. https://doi.org/10.1126/science.276.5321.2045

Raju, D. V., Ahern, T. H., Shah, D. J., Wright, T. M., Standaert, D. G., Hall, R. A., & Smith, Y. (2008). Differential synaptic plasticity of the corticostriatal and thalamostriatal systems in an MPTP-treated monkey model of parkinsonism. *The European Journal of Neuroscience*, *27*(7), 1647–1658. https://doi.org/10.1111/j.1460-9568.2008.06136.x

Reim, K., Mansour, M., Varoqueaux, F., McMahon, H. T., Sudhof, T. C., Brose, N., & Rosenmund, C. (2001). Complexins regulate a late step in Ca2+–dependent neurotransmitter release. *Cell*, *104*(1), 71–81. https://doi.org/10.1016/s0092-8674(01)00192-1

Rizor, A., Pajarillo, E., Johnson, J., Aschner, M., & Lee, E. (2019). Astrocytic oxidative/nitrosative stress contributes to Parkinson's disease pathogenesis: The dual role of reactive astrocytes. *Antioxidants*, *8*(8), 265 Retrieved from https://www.mdpi.com/2076-3921/8/8/265

Schirinzi, T., Madeo, G., Martella, G., Maltese, M., Picconi, B., Calabresi, P., & Pisani, A. (2016). Early synaptic dysfunction in Parkinson's disease: Insights from animal models. *Movement Disorders*, *31*(6), 802–813. https://doi.org/10.1002/mds.26620

Schmidt, A., Wolde, M., Thiele, C., Fest, W., Kratzin, H., Podtelejnikov, A. V., Witke, W., Huttner, W. B., & Söling, H. D. (1999). Endophilin I mediates synaptic vesicle formation by transfer of arachidonate to lysophosphatidic acid. *Nature*, *401*(6749), 133–141. https://doi.org/10.1038/43613

Shojaee, S., Sina, F., Banihosseini, S. S., Kazemi, M. H., Kalhor, R., Shahidi, G. A., Fakhrai-Rad, H., Ronaghi, M., & Elahi, E. (2008). Genome-wide linkage analysis of a Parkinsonian-pyramidal syndrome pedigree by 500 K SNP arrays. *American Journal of Human Genetics*, *82*(6), 1375–1384. https://doi.org/10.1016/j.ajhg.2008.05.005

Stevens, B., Allen, N. J., Vazquez, L. E., Howell, G. R., Christopherson, K. S., Nouri, N., Micheva, K. D., Mehalow, A. K., Huberman, A. D., Stafford, B., Sher, A., Litke, A. M., Lambris, J. D., Smith, S. J., John, S. W., & Barres, B. A. (2007). The classical complement cascade mediates CNS synapse elimination. *Cell*, *131*(6), 1164–1178. https://doi.org/10.1016/j.cell.2007.10.036

Suarez, L. M., Solis, O., Aguado, C., Lujan, R., & Moratalla, R. (2016). L-DOPA oppositely regulates synaptic strength and spine morphology in D1 and D2 striatal projection neurons in dyskinesia. *Cerebral Cortex*, *26*(11), 4253–4264. https://doi.org/10.1093/cercor/bhw263

Suarez, L. M., Solis, O., Carames, J. M., Taravini, I. R., Solis, J. M., Murer, M. G., & Moratalla, R. (2014). L-DOPA treatment selectively restores spine density in dopamine receptor D2-expressing projection

neurons in dyskinetic mice. *Biological Psychiatry*, *75*(9), 711–722. https://doi.org/10.1016/j.biopsych.2013.05.006

Südhof, T. C. (2004). The synaptic vesicle cycle. *Annual Review of Neuroscience*, *27*, 509–547.

Takei, K., Slepnev, V. I., Haucke, V., & De Camilli, P. (1999). Functional partnership between amphiphysin and dynamin in clathrin-mediated endocytosis. *Nature Cell Biology*, *1*(1), 33–39. https://doi.org/10.1038/9004

Thayanidhi, N., Helm, J. R., Nycz, D. C., Bentley, M., Liang, Y., & Hay, J. C. (2010). α-synuclein delays endoplasmic reticulum (ER)-to-Golgi transport in mammalian cells by antagonizing ER/Golgi SNAREs. *Molecular Biology of the Cell*, *21*(11), 1850–1863. https://doi.org/10.1091/mbc.e09-09-0801

Tian, J., Yan, Y., Xi, W., Zhou, R., Lou, H., Duan, S., Chen, J. F., & Zhang, B. (2018). Optogenetic stimulation of GABAergic neurons in the globus pallidus produces hyperkinesia. *Frontiers in Behavioral Neuroscience*, *12*, 185. https://doi.org/10.3389/fnbeh.2018.00185

Tomiyama, M., Mori, F., Kimura, T., Ichinohe, N., Wakabayashi, K., Matsunaga, M., & Baba, M. (2004). Hypertrophy of medial globus pallidus and substantia nigra reticulata in 6-hydroxydopamine-lesioned rats treated with L-DOPA: Implication for L-DOPA-induced dyskinesia in Parkinson's disease. *Neuropathology*, *24*(4), 290–295. https://doi.org/10.1111/j.1440-1789.2004.00559.x

Tonges, L., Frank, T., Tatenhorst, L., Saal, K. A., Koch, J. C., Szego, É. M., Bähr, M., Weishaupt, J. H., & Lingor, P. (2012). Inhibition of rho kinase enhances survival of dopaminergic neurons and attenuates axonal loss in a mouse model of Parkinson's disease. *Brain*, *135*(Pt 11), 3355–3370. https://doi.org/10.1093/brain/aws254

Tyanova, S., Temu, T., & Cox, J. (2016). The MaxQuant computational platform for mass spectrometry-based shotgun proteomics. *Nature Protocols*, *11*(12), 2301–2319. https://doi.org/10.1038/nprot.2016.136

Ungerstedt, U., & Arbuthnott, G. W. (1970). Quantitative recording of rotational behavior in rats after 6-hydroxy-dopamine lesions of the nigrostriatal dopamine system. *Brain Research*, *24*(3), 485–493. Retrieved from http://www.ncbi.nlm.nih.gov/pubmed/5494536

Verkhratsky, A., Ho, M. S., Zorec, R., & Parpura, V. (2019). In A. Verkhratsky, M. S. Ho, R. Zorec, & V. Parpura (Eds.), *Neuroglia in neurodegenerative diseases*. Springer Singapore.

Vingill, S., Brockelt, D., Lancelin, C., Tatenhorst, L., Dontcheva, G., Preisinger, C., Schwedhelm-Domeyer, N., Joseph, S., Mitkovski, M., Goebbels, S., Nave, K. A., Schulz, J. B., Marquardt, T., Lingor, P., & Stegmüller, J. (2016). Loss of FBXO7 (PARK15) results in reduced proteasome activity and models a parkinsonism-like phenotype in mice. *The EMBO Journal*, *35*(18), 2008–2025. https://doi.org/10.15252/embj.201593585

von Kriegsheim, A., Preisinger, C., & Kolch, W. (2008). Mapping of signaling pathways by functional interaction proteomics. *Methods in Molecular Biology*, *484*, 177–192. https://doi.org/10.1007/978-1-59745-398-1_12

Wang, Z., Song, Y., Zhu, W., Wang, X., Li, X., Xu, F., Si, L., Yao, T., Zhu, J., Lai, H., Li, W., Lin, F., & Wang, C. (2021). A novel FBXO7-R345P mutation in a Chinese family with autosomal recessive parkinsonian-pyramidal syndrome. *Parkinsonism & Related Disorders*, *88*, 62–67. https://doi.org/10.1016/j.parkreldis.2021.06.005

Wei, L., Ding, L., Li, H., Lin, Y., Dai, Y., Xu, X., Dong, Q., Lin, Y., & Long, L. (2018). Juvenile-onset parkinsonism with pyramidal signs due to compound heterozygous mutations in the F-Box only protein 7 gene. *Parkinsonism & Related Disorders*, *47*, 76–79. https://doi.org/10.1016/j.parkreldis.2017.11.332

Weiss, F., Labrador-Garrido, A., Dzamko, N., & Halliday, G. (2022). Immune responses in the Parkinson's disease brain. *Neurobiology of Disease*, *168*, 105700. https://doi.org/10.1016/j.nbd.2022.105700

Yalcin-Cakmakli, G., Olgiati, S., Quadri, M., Breedveld, G. J., Cortelli, P., Bonifati, V., & Elibol, B. (2014). A new Turkish family with homozygous FBXO7 truncating mutation and juvenile atypical parkinsonism. *Parkinsonism & Related Disorders*, *20*(11), 1248–1252. https://doi.org/10.1016/j.parkreldis.2014.06.024

Yang, X., Cao, P., & Südhof, T. C. (2013). Deconstructing complexin function in activating and clamping Ca^{2+}–triggered exocytosis by comparing knockout and knockdown phenotypes. *Proceedings of the National Academy of Sciences*, *110*(51), 20777–20782. https://doi.org/10.1073/pnas.1321367110

Yoo, D., Choi, J. H., Im, J. H., Kim, M. J., Kim, H. J., Park, S. S., & Jeon, B. (2020). Young-onset Parkinson's disease with impulse control disorder due to novel variants of F-box only protein 7. *Journal of Movement Disorders*, *13*(3), 225–228. https://doi.org/10.14802/jmd.20026

Zhao, Y., Qin, L., Pan, H., Liu, Z., Jiang, L., He, Y., Zeng, Q., Zhou, X., Zhou, X., Zhou, Y., Fang, Z., Wang, Z., Xiang, Y., Yang, H., Wang, Y., Zhang, K., Zhang, R., He, R., Zhou, X., … Tang, B. (2020). The role of genetics in Parkinson's disease: A large cohort study in Chinese mainland population. *Brain*, *143*(7), 2220–2234. https://doi.org/10.1093/brain/awaa167

Zou, L., Tian, Y., & Zhang, Z. (2021). Dysfunction of synaptic vesicle endocytosis in Parkinson's disease. *Frontiers in Integrative Neuroscience*, *15*, 619160. https://doi.org/10.3389/fnint.2021.619160

SUPPORTING INFORMATION

Additional supporting information can be found online in the Supporting Information section at the end of this article.

How to cite this article: Wang, J., Joseph, S., Vingill, S., Dere, E., Tatenhorst, L., Ronnenberg, A., Lingor, P., Preisinger, C., Ehrenreich, H., Schulz, J. B., & Stegmüller, J. (2023). Loss of the parkinsonism-associated protein FBXO7 in glutamatergic forebrain neurons in mice leads to abnormal motor behavior and synaptic defects. *Journal of Neurochemistry*, *167*, 296–317. https://doi.org/10.1111/jnc.15962